Initial Determination of Low Earth Orbits Using Commercial Telescopes

THESIS

Matthew M. Schmunk, Captain, USAF

AFIT/GA/ENY/08-M11

AFIT/GA/ENY/08-M11

Initial Determination of Low Earth Orbits Using Commercial
Telescopes

THESIS

Presented to the Faculty

Department of Aeronautics and Astronautics

Graduate School of Engineering and Management

Air Force Institute of Technology

Air University

Air Education and Training Command

In Partial Fulfillment of the Requirements for the

Degree of Master of Science in Astronautical Engineering

Matthew M. Schmunk, BS

Captain, USAF

March 2008

APPROVED FOR PUBLIC RELEASE; DISTRIBUTION UNLIMITED

INITIAL DETERMINATION OF LOW EARTH ORBITS USING COMMERCIAL
TELESCOPES

Matthew M. Schmunk, BS

Captain, USAF

Approved:

_____   _____
Dr. Richard G. Cobb (Chairman)   Date   12 MAR 08

_____   _____
Lt Col Nathan A. Titus (Member)   Date   12 Mar 08
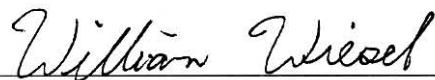
_____   _____
Dr. William E. Wiesel (Member)   Date   12 March 08

AFIT/GA/ENY/08-M11

Abstract

Within the last decade, many new technologies have significantly changed the face of private astronomy. Developments such as inexpensive but high-quality sensors, rapid personal computing, and easy networking inspire a reexamination of an old problem: how practical is it to develop initial orbit estimates for Low Earth Orbiting (LEO) satellites using optical tracking? This paper documents the design and implementation of a commercial telescope system used to answer precisely that question. This analysis determined there are some challenging barriers to successful single-site orbit determination, but it is possible given the right conditions. Considering the low cost and small support footprint of such systems, they could provide excellent support to Space Situational Awareness (SSA) missions or satellite tracking operations in general.

Acknowledgements

Many thanks are offered to the friends and classmates that volunteered their early mornings and late evenings to help collect data. They braved cold weather, hardware errors, software malfunctions, and an often-exasperated researcher. I offer special recognition to those that helped me understand those exasperating problems: Robert Matson, Richard Seymour, and Dr. William Wiesel deserve particular credit. Finally, my father deserves the greatest acknowledgement - he first saw the ECHO satellite drift brightly in the night sky during training at Fort Riley, Kansas in the late 1950s. He could not have imagined a camera lens he bought in Germany a few years later would be used in an Air Force research project half a century beyond. His support (and ready ability to lend tools, hardware, and advice) over the years is greatly appreciated.

Matthew M. Schmunk

Table of Contents

List of Figures

List of Tables

List of Symbols

List of Abbreviations

Abbreviation		Page

Initial Determination of Low Earth Orbits Using Commercial Telescopes

I. Problem Statement

R APID advances in the quality of electronics, combined with equally dramatic improvements in cost and availability, are revolutionizing private astronomy. Unparalleled access to quality equipment, rapid personal computing, and extensive community support enable nearly anyone to achieve feats in their backyard that required an observatory twenty years ago. Semi-professional astronomers and programmers continually develop novel, inexpensive methods to defeat complex engineering challenges.

One such challenge is optically tracking satellites to determine their orbits. There are long-standing solutions, but this project approaches it with refreshed interest. Primary motivations include:

- Space Situational Awareness (SSA): Commercial systems are inexpensive, mobile, and easily supported: all factors that compensate for limitations in capability. There are always new opportunities to use them for surveillance and debris monitoring.

- State-of-the Art Survey: This study offers a baseline explanation of methods used by semi-professional satellite observers today. Hopefully, it will serve as a reference for future researchers and motivate them to pursue additional work in this field.

- Research Testbed: By its conclusion, this project integrated the hardware and software required to operate a basic optical satellite tracking program. Now, students may use it to support work in sensors, image processing, orbit determination, and many other fields. It also allows AFIT students to gain hands-on experience with classroom concepts.

Tracking artificial satellites is a pastime as old as the Space Age itself. Like many other subdisciplines of astronomy, this field benefits greatly from recent advances. This project examines how modern equipment is used to track Low Earth Orbit (LEO) satellites in order to determine their orbits.

Successful determination of any body's orbit requires accurate measurements in both space and time. For millennia, astronomers had no way of estimating how far away stars and planets were, so the methods they developed for predicting their positions relied only on time and relative angular measurements. Great minds of the day (namely Gauss and Laplace) developed very robust routines for calculating orbits with such data. Today, these methods are collectively called "angles only" techniques.

When artificial earth satellites were first launched in the late 1950s, they brought with them a pressing need for accurate orbital measurements. Without them, it would be impossible to keep track of a launched satellite. Astronomers implemented familiar angles only methods to monitor these new celestial bodies, yet they would face unique new challenges. Chapter II describes the origins of optical satellite tracking and enumerates key data needs for successful orbit determination. It also describes how, using fundamental principles established decades ago, it is possible to apply modern computing, imaging, precision navigation, and timing technology to produce effective results at low cost. Chapter II concludes with a brief overview of the hardware and software selected for this project.

Chapter III discusses the prerequisite task of identifying opportunities for visual satellite tracking. First, the North American Aerospace Defense Command (NORAD) satellite catalog is discussed, followed by an overview of the SGP4 algorithm used to extract orbits contained in the catalog. Then, key transformations between local and inertial frames are described in detail. Finally, satellite brightness models are applied. Once these steps are complete, it is possible to pursue observations with a high certainty of success.

Chapter IV explains how collected data is processed to produce local angular measurements of satellite overflights. Then, these measurements are transformed to an inertial reference frame in preparation for initial orbit determination.

The results of system calibration and early observations are presented in Chapter V. A case study is presented that reveals this system is capable of producing useful initial orbit estimates, given the right conditions. There are numerous theoretical and practical concerns that complicate tracking with a single telescope from a single site. Considering the low cost of systems like this, however, these complications may become irrelevant if multiple sensors are employed.

Chapter VI summarizes the project and expands on the initial conclusions determined in this course of study. It identifies specific research areas that deserve further analysis, in order to both deepen understanding of optical tracking and build a foundation future tracking networks can rest on.

II. Background

FROM the ground, an observer can spot sunlight reflecting off of a satellite under the right conditions, much like sunlight reflects off the moon. This means a satellite can appear as bright as a star, with the notable exception that it moves much faster across the night sky.

In October of 1957, this effect caused great concern in the United States as the world's first artificial satellite, Sputnik 1, could easily be seen flying methodically over-head. The shiny metal sphere's polish went beyond propaganda - its mirror-like surface aided telescope tracking [*Smithsonian*, 2008]. The probe's radio beacon had a limited lifespan, and only one radar in England was capable of tracking the relatively large rocket body that remained in space, not Sputnik itself [*BBC*, 2007].
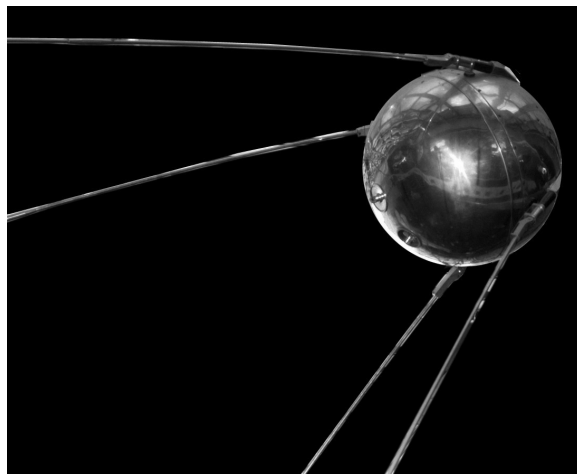
Figure 2.1:   Sputnik 1 [*NASA*, 2007]

Shortly before Sputnik's launch, the Smithsonian Institution organized *Operation Moonwatch*. Its international observer corps first tracked Sputnik, then other satellites over many years that followed. Volunteers used arrays of very simple instruments to record the time and place a target satellite passed a given observing site. These measurements were used to calculate satellite orbits and also determine geophysical properties of the Earth and its atmosphere.[1]

---

[1]For a thorough and delightfully campy history of the early days of satellite tracking, refer to [*Engle and Drummond*, 1965].

AN AUSTRALIAN *Moonwatch Team is part of a world wide group of volunteer observers who have made over 100,000 valuable observations of satellites. Moonwatch observers can compete with photographic and radar stations especially on very low altitude fast moving objects. They have proven to be a necessary part of the satellite tracking program.*

—Smithsonian Astrophysical Observatory
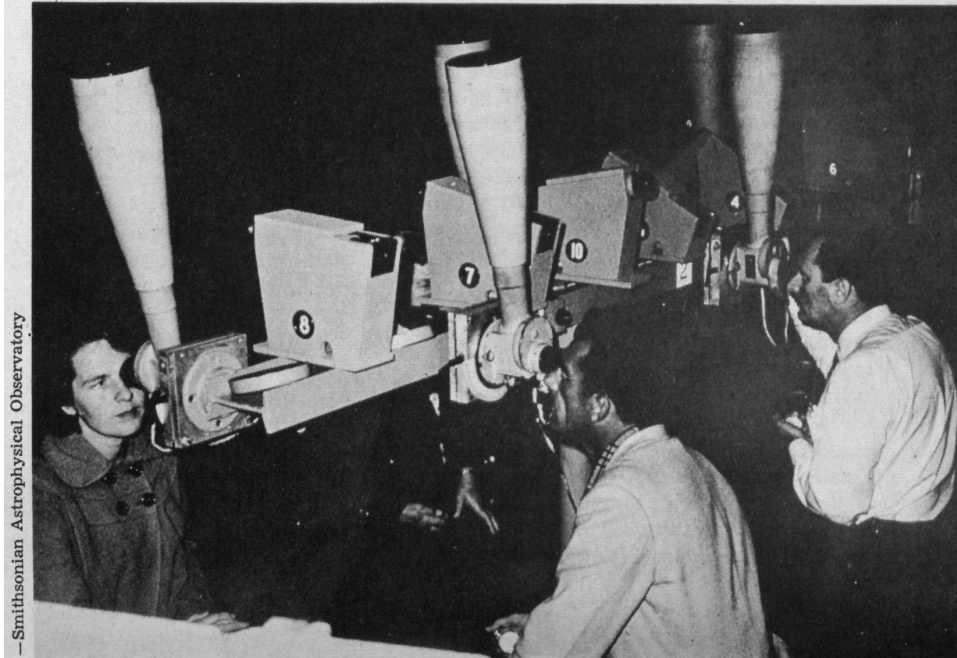
Figure 2.2:   Australian Project Moonwatch Volunteers (*Photo Courtesy the Harvard-Smithsonian Center for Astrophysics*)

As the U.S. government developed a comprehensive satellite tracking network, however, the role of optical tracking changed dramatically. Large sky-scanning radars were developed that could find and measure objects in LEO regardless of sky conditions. Additionally, radars can determine range and instantaneous change in range (range-rate) to the target. Because of this, telescopes' missions narrowed. Today, the Ground-Based Electro-Optical Deep Space Surveillance (GEODSS) system is used to observe objects beyond radar range, developing orbits for objects 10,000 to 45,000 kilometers from Earth. GEODSS telescopes have a one meter diameter and use a Charge-Coupled Device (CCD) camera to detect objects 10,000 times dimmer than visible with the naked eye [*USAF*, 2006]. Undoubtedly, GEODSS is many times more capable than its predecessors, and represents the technological peak of optical satellite tracking.

Two other government-sponsored systems are noteworthy as well, because they use commercial equipment to track and analyze satellites. The United States uses the *Raven* system to support its space tracking efforts, including satellite and debris characterization

and tracking in all orbital regimes [*Kervin et al.*]. The Canadian Satellite Tracking and Orbit Research (CASTOR) has stated objectives to bring amateurs and professionals together, and performs varied missions as well. In honor of Sputnik's 50th anniversary, CASTOR tracked over 2000 distinct objects in 2007 [*Earl*, 2008]. Both systems are now in service for over a decade.

Whether using a simple or sophisticated telescope, their fundamental purpose in orbit determination is the same: accurately measure the apparent position of a target at a specific time. The remainder of this chapter discusses bedrock concepts that help reach that seemingly simple goal. Since this project deals exclusively with observing satellites in the visible range, Section 2.1 describes how astronomers describe the brightness of a celestial body. Section 2.2 describes what theoretical parameters are required to develop orbits using telescope data, followed by a section on major sources of potential error. Finally, Section 2.3 provides a brief overview of modern techniques used to eliminate major observational errors and explains the equipment used in this study.

2.1 The Visual Magnitude Scale

Quantifying the brightness of nighttime objects is hardly a recent pursuit. The ancient Greek astronomer Hipparchus developed a catalog of stars' intensities by subjectively placing any one he could see into one of six categories. Ptolemy would continue the tradition of referring to the brightest stars as first magnitude, whereas sixth magnitude stars were barely perceptible [*Kennon*, 1948]. Despite two millennia of scientific advance, this terminology and the concept of apparent magnitude remains embedded in the *lingua franca* of astronomy. The following concepts are critical:

- Higher is Lower: Unlike most scientific scales, brighter objects have numerically *lower* apparent magnitudes, extending into the negative range.

- Logarithmic Scale: A decrease of one in apparent magnitude (say, 5 to 4) corresponds to a $\sqrt[5]{100} \approx 2.512$ multiplication in brightness. This ratio was proposed by Norman Pogson as a standard in 1856 [*Pogson*, 1856]. To express any scalar multiple in apparent magnitude (M_x) as a common logarithm, the following change

of base is used:

$$\log_{(\sqrt[5]{100})}(M_x) = \frac{\log_{10}(M_x)}{\log_{10}(\sqrt[5]{100})} = 2.5\log_{10}(M_x) \qquad (2.1)$$

The apparent magnitude's logarithmic scale is well suited for the human eye's logarithmic visual response curve. Other sensors, such as film or CCD cameras, respond differently. Refer to [*Rees*, 2001] for an introduction to remote sensing methods that take sensor performance into account.

- Absolute Magnitude: A reference brightness called *absolute magnitude* defines an object's brightness if observed at a standard distance and orientation. Depending on the desired correction, an apparent magnitude may be predicted for a given geometry[*Pogson*, 1856; *Meeus*, 1998].

Pogson is credited with creating the modern visual magnitude scale. During his time, astronomers were searching for a suitable model to predict the brightness of asteroids. Pogson claimed his formula could accurately match observed trends, and that any errors would be constant. He predicted this constant error would be caused only by his mis-estimation of each body's absolute magnitude; he then boldly notes "but this I do not anticipate" [*Pogson*, 1856]. This philosophy is simple: pick a model that matches trends and adjust the bias (in this case absolute magnitude) to match observations.

A century later, F.L. Whipple and J.A. Hynek calculated apparent magnitude estimates for orbiting satellites as they designed the United States' first tracking telescope network. They presented their working assumptions to the Institute of Radio Engineers:

> Calculations show that at a zenithal distance of about 200 miles in twilight a 20-inch sphere with albedo 0.6 would have a photographic magnitude of 6.3 and a visual [apparent] magnitude of 5.7. [*Whipple and Hynek*, 1956]

The exact calculation and assumptions they used are undocumented, but Chapter III, Section 3.3 will describe how methods much like those Pogson and Whipple employed are still in use today.

2.2 Angles Only Orbit Determination

Orbit solutions that do not use target range data are collectively called angles only methods. They are the oldest class of solutions, born out of a necessity to evaluate early astronomical observations based only on the relative angular positions of wandering planets against an unchanging starfield. Dr. Pedro Ramon Escobal provides an introduction to such methods in his 1965 text *Methods of Orbit Determination*. He notes,

> [T]he angles only problem attracted the attention of both Gauss and Laplace. In their day, this was one of the most pressing problems in mathematical astronomy. Today, a century and a half later, these methods are widely utilized and, in short, have stood the test of time.[*Escobal*, 1965]

Should the reader need a complete explanation of angles only methods or common celestial coordinate systems, refer to Escobal's text. The rest of this section explains only the basics, because they greatly influence instrument design.

Since most orbit equations of motion use the Earth Centered Inertial (ECI) frame, all measurements must be converted accordingly. For a fixed ground observer, the following parameters are required to accomplish this:

- Local Sidereal Time (LST): Since Babylonian times, star's longitudes on the celestial sphere are represented sexigesimally in hours, minutes, and seconds from an arbitrary point (the vernal equinox). A site's LST is the celestial meridian that lies directly overhead at any instant in time. To reinforce the fact this quantity is an angle and not time as commonly known, LST is referred to as the angle θ.

- Latitude and Longitude: These parameters are required in a number of vector transformations, discussed in detail later.

- Altitude: This parameter allows minor geometric corrections to the basic oblate Earth model employed in transformation calculations.

- Target Azimuth and Elevation: If all previous parameters are available, a measurement in the local horizon, or South-East-Zenith (SEZ) frame, may be converted to an inertial one.

To develop an initial orbit estimate, position vectors are required. Gauss developed a method of accomplishing this given only three line-of-sight vectors and their corresponding times.[2] If more than three vectors are available, there are a number of algorithms that can improve solution accuracy. Longer arcs between points are also desirable [*Escobal*, 1965].

In principle, angles only orbit determination is simple. Tasks that are simple in theory, however, often become complex in execution. The following section explores a number of complicating factors.

2.3   System Architecture and Instrumentation

Section 2.2 provided a short list of data needs for angles only orbit determination. This section describes the system designed for this project, assumption rationale, and other useful background items. The architecture used in this study is summarized in Figure 2.3. Basic hardware descriptions follow, whereas specific calculations and software components are laid out in subsequent chapters.
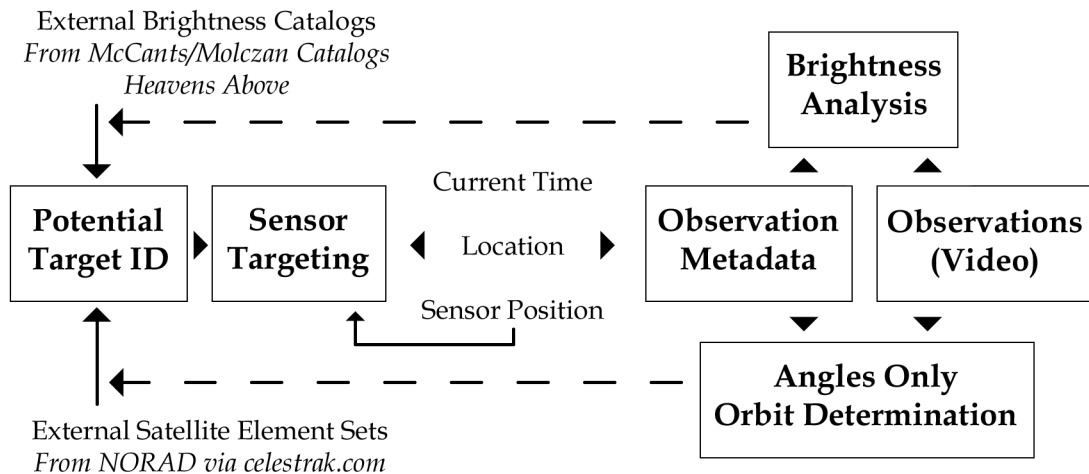
Figure 2.3:   Angles Only Orbit Determination Architecture

---

[2]The "angles" in angles only refers to the angles between line-of-sight vectors in the orbit plane. In practice, the orbit is inclined from the coordinate frame, so an additional angle for each measurement is required in order to determine the orbit plane orientation. Therefore, a pair of angles (in this study azimuth and elevation) is required to compute each line-of-sight vector.

Before continuing to descriptions of specific hardware and software elements that will fill the architectural needs shown in Figure 2.3, an important question must be addressed: what precision and accuracy is required to complete the task at hand? For this system, as with any instrument design, unbiased and random (i.e. Gaussian) errors are desirable. In his book *Modern Orbit Determination*, William Wiesel states that,

> In practice, [Gaussian distribution] is achieved by finding *and eliminating* all of the large error sources in an instrument, until the point of diminishing returns is reached. The remaining error sources will be many in number, and small in size, and the central limit theorem will be obeyed. [*Wiesel*, 2003]

Those familiar with experimental research know all to well how often equipment fails as a white noise generator, however. To effect successful data collection, some understanding of the instrument at hand is required. This ensures suitable reference frames are selected and appropriate precautions taken throughout the design process.

Since this thesis examines commercial telescopes, some aspects of the architecture are predetermined. For this project, a homemade imaging camera was used in conjunction with a popular commercial telescope, the Meade LX200GPS (Figure 2.4).
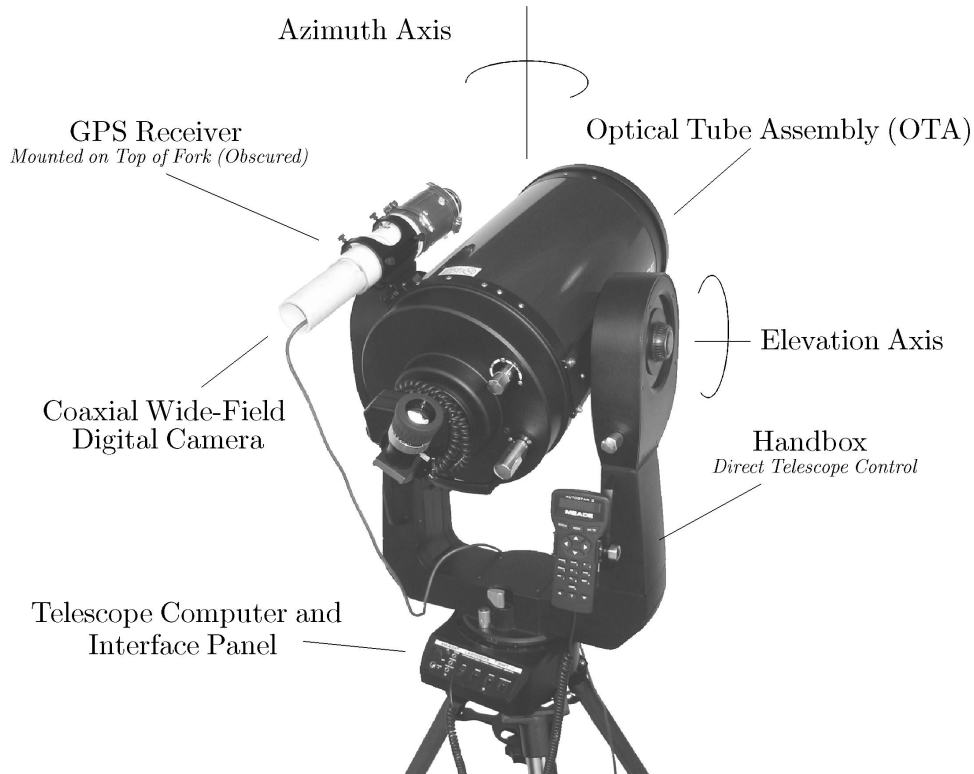
Figure 2.4:   Meade LX200GPS Telescope

This telescope includes a number of modern features, most notably:

- Global Positioning System (GPS) Receiver: Inexpensive receiver chips have revolutionized hobby astronomy, quickly calculating accurate time, latitude, longitude, and altitude data.

- Onboard Computer: The computer processes GPS data, controls axis servomotors, applies tip, tilt, refraction, and other corrections, and has a large internal database of celestial objects. The telescope's computer communicates with a personal computer via an RS232 interface, using a command set provided by the Meade Corporation [Meade, 2003].

- Digital Video Camera: A wide variety of digital cameras may be used either through the telescope's main optics, or coaxially mounted to the telescope's Optical Tube Assembly (OTA). The Universal Serial Bus (USB) architecture is commonly used to both power the sensor and transmit images.

In many respects, a telescope is only as good as its mount. This is especially true if an operator (or a computer) needs reliable attitude references in order to find targets, track them, or extract measurements. Azimuth-elevation (or Az-El) mounted telescopes like the Meade LX200GPS are very popular for all these reasons. Whether using internally-generated calculations or following ones from an external source, the telescope's onboard computer can independently command axes servomotors to recreate any arc across the sky. For astronomical purposes, this is required to track heavenly bodies at a sidereal rate.[3] Azimuth-elevation telescopes also suffer from a phenomenon known as *field rotation*. Objects appear to orbit around a sidereally-tracked center point in the image plane; the effect gets worse further out. The effect is noticeable when performing long-exposure astrophotography, but is inconsequential for exposures on the order of seconds or even minutes.

Just as it tracks stars, an az-el telescope can also follow satellites across the sky. The Meade LX200GPS allows users to upload satellite element sets, after which the computer propagates their orbits and tracks them at the appropriate time. This allows owners to experience the "exciting challenge" of satellite observing [*Meade*, 2003]. If the equipment is operating properly, the satellite remains stationary in the sensor's field of view as stars go whizzing by behind it. In theory, observation functions for this kind of data could produce accurate angular measurements.

Imagine the following, however: in an American football game, the ball's position is recorded after every play. Lines are painted on the field to help the referees estimate where it stopped, and when necessary, chains are used to measure distances accurately. The hopes and dreams of millions of fans sometimes depend on these measurements. Now imagine a game in which the referees can only watch the ball through telephoto lenses from the top of the stadium, they must keep the ball centered, and the ball never stops moving. Placing the ball's position this way is hardly ideal, just as measuring a

---

[3]A sidereal rate is one revolution per sidereal day, which is $\approx 1/365$ shorter than a solar day. A traditional equatorial (or polar) mount aligns the telescope with constant lines of celestial latitude, so it need rotate in only one axis to keep a star centered in the field of view. Gimballed mounts achieve the same for satellites, where the telescope is first aligned with the overflight's arc, then is panned either left or right at the appropriate angular rate. Az-El telescopes must translate in both axes to achieve the same goal, so complex interpolations are required.

satellite's position against a moving background is equally difficult. Every measurement requires a reference: for this system, a relatively stationary starfield will do nicely.

By astronomical standards, this project uses a relatively wide-field digital camera. This serves two purposes: a) it is more forgiving of targeting or timing errors, and b) any given image will be more likely to have reference stars in it. This is critical, because mobile systems like this one behave differently during every sortie. Although care is taken to mitigate most major errors, it is impossible to remove every misalignment that may occur. Since stars have very well-known positions, any collected image may be realigned using astrometric principles. Details are provided in Chapter V.

The wide-field camera used in this project is a simple device, built from a Logitech 3000 webcam and a vintage Single Lens Reflex (SLR) camera lens. The SLR lens, a 35mm Schneider-Kreuznach f/2.8, would normally produce very wide ($\approx 70°$) fields of view when used in conjunction with 35mm film. However, when placed in front of the webcam (with its original lens removed), there is significant magnification: the webcam's chip is a fraction of the size of 35mm film. The camera lens is positioned in front of the webcam aperture so that the system has approximate focus, and fine adjustments are made using the focus ring on the SLR lens. Conveniently, both the webcam and lens fit neatly in standard two inch PVC pipe, which also matches the guide scope mount on the OTA. No great effort was spent designing the sensor, but the following parameters are empirically determined from using it in practice:

Table 2.1:   Wide Field Camera Parameters

Field of View (4:3):	5.7° / 4.73°
Image Size [pixels]:	640×480
Framerate [fps]:	5
Lower Apparent Magnitude:	≈ 6

It is desirable to provide a recognizable starfield reference, yet avoid complications caused by a moving telescope such as vibrations or poor tracking performance. Therefore, this project adopts a slew-and-shoot method: a single sensor achieves hemispherical sky coverage by riding on a precisely aligned telescope. The telescope leads the target, pausing in anticipation of an intercept. By the time data is collected, the scope is

no longer moving. This method may also be directly applied to permanently mounted cameras, either singly or in a cluster configuration. Regardless of the sensor setup, each data collect (in this case video) must have the corresponding metadata:

- Time: Each video frame's collection time enables precise dynamic measurements. Since video systems have relatively accurate framerates, only the video's start time must be logged. Subsequent times are determined by multiplying the inverse of the framerate by the number of frames elapsed since video start. This method assumes times are logged in UTC time, then converted to Julian Dates using Equation 3.4.

- Site Location: For a stationary observer, site parameters must be logged only once per observing session. They are used to determine the site's inertial position as discussed in Chapter III.

- Sensor Altitude and Azimuth: The telescope's reported attitude in terms of compass azimuth (A) and elevation above the horizon (h) is recorded for each video.

This document does not include an exhaustive analysis of how observational errors are dealt with in orbit solutions - refer to Wiesel's text for a more complete analysis. Still, mitigating such errors is important and a robust system must account for them. The following items are are primary areas of concern, presented here because they lurk behind every calculation in this examination.

- Errors in Time: Because time is critical to the transformation of observations from local to inertial frames, access to accurate time data is of foremost concern.

- Errors in Observer Position: Without an accurate understanding of the observer's position on the Earth, local (SEZ) to inertial (ECI) transformations are not possible. Furthermore, some corrections for orientation depend on accurate position data.

- Errors in Telescope Orientation: If an instrument is not perfectly aligned with its assumed reference frame, a variety of errors may occur. For a ground-based telescope, there are two basic but important corrections:

– Earth oblateness: If the Earth were a perfect sphere, a site's global latitude would directly correspond to a line of celestial latitude. Due to centripetal acceleration, however, the Earth bulges at the equator. Unless the observer is precisely on the equator or at one of the poles, a minor correction is necessary.

– Tip and tilt: Errors occur when an a calculated local zenith vector does not match the true zenith vector. Generally speaking, these occur when the telescope mount is not level.

• Sensor Errors: Whether looking through an eyepiece or using a camera, misalignments or rotations in optical systems induce additional errors. Although not an error per se, the effects of atmospheric refraction must also be accounted for when interpreting sensor data.

Through careful system design these errors can be greatly diminished, resulting in quality observations, as shown in Chapter V. Appendix A explains some hardware-unique issues encountered in this project.

III. Predicting Visible Satellite Overflights

SIMPLY put, the sky is very large and satellites are very small. To make matters worse, most telescopes have relatively narrow fields of view. Colloquially, this is referred to as looking through the "soda straw." Setting up a telescope and waiting for something to fly across its field of view would waste many clear nights. This chapter describes how to guide a sensor to appropriate targets given a catalog of satellite element sets and brightness data. Although the ultimate goal is to generate orbits from measured data without such inputs, solving this inverse problem first reveals many fundamental concepts. Figure 3.1 depicts the elements that are necessary to find and track visible satellites.

External Brightness Catalogs
From McCants/Molczan Catalogs
Heavens Above

| Brightness Model | Current Time | | } | Observation Metadata |

Location   Sensor Position

| Potential Target ID | ECI to SEZ Frame | Sensor Targeting | ▶▶▶ | Observations (Video) |

| SGP4 Propagator |

External Satellite Element Sets
From NORAD via celestrak.com
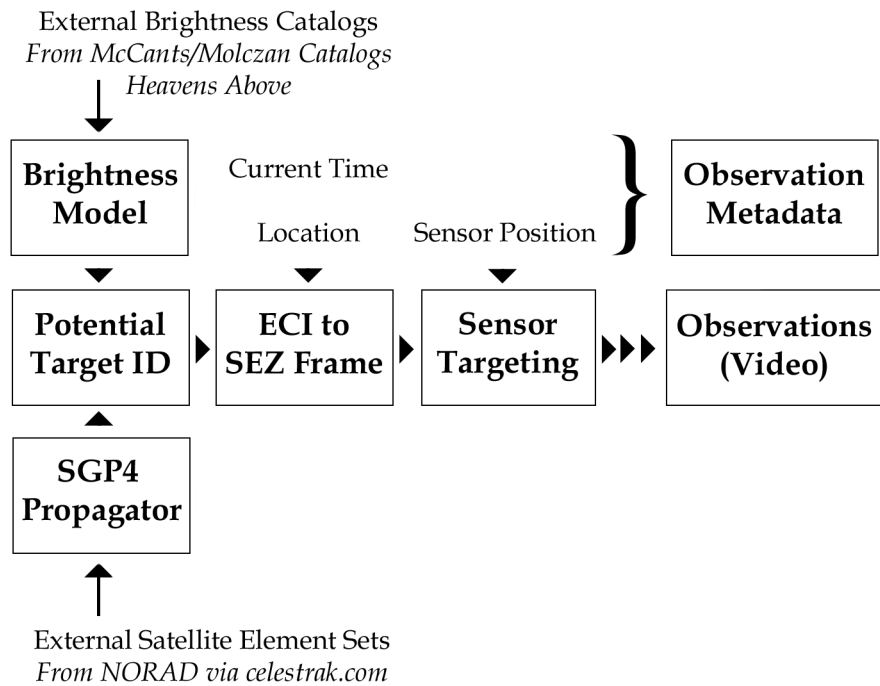
Figure 3.1:   Steps to Predict Bright Satellite Overflights

Predicting when satellites will be visible requires a) knowing where the satellite is, b) knowing where the observing site is, and c) estimating how bright the satellite will be. Sections 3.1 through 3.4 explain the methods and mathematics required to identify bright satellite passes. Section 3.5 showcases the integrated tracking software that was developed during this project.

3.1 Satellite Catalogs and Orbit Prediction

From this point forward, the term *satellite* is used in its purest sense, that is to refer to any body orbiting the Earth. A casual glance at the NORAD catalog reveals most tracked objects never were or no longer are active craft. Even so, "what goes up must stay up" when dealing with orbital velocities, so without propulsion or control many will remain in orbit for decades or centuries. In this sense, NORAD is the curator for a rapidly spinning museum, making periodic rounds to ensure each artifact is properly labeled. Generally speaking, objects tracked during this research project have long since passed from the centerfolds of trade magazines. Discriminating active from inactive objects is also well outside the scope of this work.[1]

Predicting overflights requires knowledge of any given satellite's inertial position at any given time. First, a reference estimate of the satellite's orbit at some particular time (or epoch) is required. These are called element sets, or with NORAD data in particular a Two Line Element Set (TLE). Then, a means of propagating that estimate forward is necessary, subject to appropriate equations of motion and perturbations.

To use NORAD TLE data, the Simplified General Perturbations-4 (SGP4) model is used. Comprehensive descriptions of the method are available in [*Vallado et al.*, 2006] and [*Hoots et al.*, 1988], so there is little need to belabor the details here. Both TLE data and source code in various formats is available through Dr. T.S. Kelso's website *celestrak.com* [*Kelso*, 2007].

This project uses a MATLAB® version of the SGP4 routine as adapted by Jeff Beck from code originally written by David Vallado.[2] It is further modified to be "vectorized," that is all loop operations were replaced with matrix algebra operations.[3] This improves calculation time by about a factor of 16, allowing much better realtime overflight computation.

---

[1] Rapidly tumbling objects exhibit visible flash periods, so it is possible to declare them out-of-control in some cases.

[2] MATLAB® is a registered trademark of The MathWorks, Inc.

[3] The one exception is the solution of Kepler's Equation, which is normally solved through iteration. In this case, each element's corrections are computed simultaneously once per loop, then individually frozen from future updates as soon as they reach convergence. This ensures results match the published validation cases included in [*Vallado et al.*, 2006].

The SGP4 algorithm ultimately produces an inertial position and velocity vector for any satellite in question. These vectors are referred to as $\vec{r}_{sat}$ and $\vec{v}_{sat}$ in subsequent calculations.

3.2 Site Parameters and Overflight Prediction

Once a satellite's inertial position vectors are available, half of the overflight problem is solved. The second part involves doing the same for the ground site. Fortunately, the dynamics are much simpler. This section describes the required transformations that conclude with the determination of when and where any given satellite will be visible to the observer.

Of all the required parameters in the following transformations, the most important is accurate time. This problem is greatly simplified by using a GPS receiver. Most varieties provide Universal Coordinated Time (UCT) or Zulu (Z) time. Using any readily-available formula, such as the one included in the Aerospace Toolbox for MATLAB®, UCT is converted to Julian date (JD). Determining JD is key, because first it connects us to satellite orbit predictions, and secondly helps determine our ground site's inertial position.

To transform from the Earth Centered Rotating (ECR) frame to the ECI frame, Greenwich Apparent Sidereal Time (GAST), expressed with the angle θ_g, is required. This angle is measured positive eastward between the vernal equinox and the Prime Meridian, i.e. the location of Greenwich, England. For a given time, θ_g is calculated using a United States Naval Observatory (USNO) algorithm. First, a Greenwich Mean Sidereal Time (GMST) is found using:

$$D = JD - 2451545.0$$

$$GMST = 18.697374558 + 24.06570982441908 D \qquad (3.1)$$

Then, a correction for nutation in right ascension is applied, using a formula called the *Equation of the Equinoxes (eqeq)*. First, approximations for Mean Longitude of the Sun

(L) and Longitude of the Ascending Node of the Moon (Ω_{Moon}) are used to determine the Nutation in Longitude ($\Delta\psi$).

$$L = 280.47 + 0.98565D$$

$$\Omega_{Moon} = 125.04 - 0.052954D$$

$$\Delta\psi \approx -0.000319\sin(\Omega_{Moon}) - 0.000024\sin(2L)$$

After calculating obliquity (ε),

$$\varepsilon = 23.4393 - 0.0000004D$$

The correction term *eqeq* is found from

$$eqeq = \Delta\psi\cos(\varepsilon) \tag{3.2}$$

Finally,

$$\theta_g = GMST + eqeq \tag{3.3}$$

For this and any following angle calculations, the resulting answer is converted to decimal degrees and wrapped to its appropriate domain, in this case $[0°, 360°)$. According to the USNO, Equation 3.1 loses one arcsecond ($\approx 1.2e^{-5}$ degrees) per century. If correcting with Equation 3.2, a maximum error of 0.432 arcseconds and a root-mean-square (RMS) error of 0.01512 arcseconds is expected [*USNO*, 2007b, 1981]. An updated method is available in [*Kaplan*, 2005], but the method presented here is more than sufficient for the selected application.

For a stationary observer, a site's latitude, longitude, and elevation must be determined only once per observing session. Any GPS receiver provides the following information:

- Longitude: Manufacturer's conventions vary, so care should be taken determining which hemisphere corresponds to a positive angle. For an East longitude λ_E

(measured positive eastward from the Prime Meridian), the site's Local Apparent Sidereal Time (LAST, or θ_{site}) is easily calculated:

$$\theta_{site} = \theta_g + \lambda_E \qquad (3.4)$$

- Latitude: Receivers report geodetic (map) latitude ϕ, which is used in determining a site's ECI position vector (Equation 3.6), the ECI-to-SEZ transformation (Equation 3.17), and the SEZ-to-$I_t J_t K_t$ transformation (Equation 4.2) [*Escobal*, 1965; *Vallado and McClain*, 2007].

- Altitude: Terrestrial navigation references altitude above Mean Sea Level (MSL), but sea level and the Earth's reference ellipsoid are not coincident. Most GPS receivers report altitude above MSL (H_{MSL}) as well as the height of its sea level model above or below the ellipsoid (H_{geoid}). The receiver's height above the reference ellipsoid, H, is then:

$$H = H_{MSL} + H_{geoid} \qquad (3.5)$$

Once time and navigational position are known, the site's ECI position vector may be determined using Equation 3.6 to calculate $\vec{r}_{site}$.[4] The mean Earth radius a_e and flattening parameter f are calculated from precise worldwide measurements. GPS uses the World Geodetic System 1984 (WGS-84) survey as a reference frame. Because f is very small, the WGS-84 standard provides its inverse [*NIMA*, 2000]. Two preliminary values are calculated: the first is eccentricity squared (e^2) followed by the radius of curvature in the prime vertical (N).

$$e^2 = 2f - f^2$$

$$N = \frac{a_e}{\sqrt{1 - e^2 sin^2(\phi)}}$$

---

[4]This is a very common transformation from the geodetic to the ECR frame with a positive counter-clockwise rotation about the Earth's axis by θ_{site}. The ECR transformation and other practical GPS resources are referenced at [*Dana*, 2000].

$$\vec{r}_{site,ECI} = \begin{Bmatrix} X_{site} \\ Y_{site} \\ Z_{site} \end{Bmatrix} = \begin{Bmatrix} (N+H)\cos(\theta_g)\cos(\phi)\cos(\lambda_E) - (N+H)\sin(\theta_g)\cos(\phi)\sin(\lambda_E) \\ (N+H)\sin(\theta_g)\cos(\phi)\cos(\lambda_E) + (N+H)\cos(\theta_g)\cos(\phi)\sin(\lambda_E) \\ (N(1-e^2)+H)\sin(\phi) \end{Bmatrix}$$

(3.6)

Of course, if a site's parameters are well known, a position vector may be calculated at any arbitrary time. This is required when generating future predictions.

At this point, both the site and satellite's position vectors are available. With this data alone it is possible to apply what could be called a binary brightness model; this model's main parameter involves transmission losses due to the amount of earth between the observer and satellite. Plainly speaking, simple checks are made to determine if the satellite is above the local horizon or not. Let us define a line-of-sight vector $\vec{r}_{LOS}$ between the site and satellite,

$$\vec{r}_{LOS} = \vec{r}_{sat} - \vec{r}_{site}$$

Also, determine a unit vector that points towards zenith in the ECI frame ($\hat{\vec{z}}$) as a function of ϕ and θ_{site}:

$$\hat{\vec{z}} = \begin{Bmatrix} \cos(\phi)\cos(\theta_{site}) \\ \cos(\phi)\sin(\theta_{site}) \\ \sin(\phi) \end{Bmatrix}$$

Finally, using the definition of the dot product, the zenith angle z may be calculated.

$$z = cos^{-1}\left(\frac{\hat{\vec{z}} \cdot \vec{r}_{LOS}}{|\vec{r}_{LOS}|}\right)$$

(3.7)

At this point, elevation from the local horizon h is substituted, where $h = 90° - z$. Using h, Equation 3.7, and either a loop or vector of time, overflight occurrences are quickly calculated. If desired, a simple logical inequality can compare results to a minimum threshold, say $10°$ above the horizon, and disqualify any pass that fails to break this point.

This method may also be used to calculate sunrise and sunset. The Jet Propulsion Laboratory (JPL), through their HORIZONS online interface, provides information on over 40,000 solar system objects. The system can produce position vectors between any two bodies between selected times [*JPL*, 2008]. Using Equation 3.7 and the Sun's ECI position vector $\vec{r}_{Sun}$, its zenith angle is determined. Since standard definitions of sunrise, sunset, and twilight are only a function of zenith angle, these times are easily determined [*USNO*, 2007a].

The Sun's position vector serves a second purpose, as well. Although popular media often portrays satellites as beeping behemoths covered in bright blinking lights, this is sadly not the case; they emit no visible light of their own. The following method determines whether or not a satellite is directly illuminated by the sun, using a very simple model that treats the Earth's shadow as an infinitely long cylinder of Earth's radius. First, the acute angle between the Sun and satellite vectors, $\eta_{Sun,sat}$ is found:

$$\eta_{Sun,sat} = cos^{-1}\left(\frac{\vec{r}_{Sun,ECI} \cdot \vec{r}_{sat,ECI}}{|\vec{r}_{Sun,ECI}||\vec{r}_{sat,ECI}|}\right) \tag{3.8}$$

If $\eta_{Sun,sat} = 0°$, the satellite is directly between the Sun and the Earth. Conversely, $\eta_{Sun,Sat} = 180°$ indicates the Earth is directly between the Sun and satellite: the satellite is in total darkness. The maximum angle at which the satellite falls outside the Earth's shadow (η_{max}) is a function of the satellite's distance from Earth,

$$\eta_{max} = \cos^{-1}\left(\frac{a_e}{|\vec{r}_{sat}|}\right) + 90° \tag{3.9}$$

At any time $\eta_{Sun,sat}$ from Equation 3.8 is greater than the angle computed in Equation 3.9, the satellite falls within the Earth's shadow.

By applying these simple, rapidly-calculated checks the number of potential targets is dramatically reduced. Only satellites that have direct lines of sight to both the Sun and the site in question remain, so the basic overflight question is answered. These targets are only *potentially* visible, however. The following section describes how to further improve observations by generating an estimate of each satellites' brightness.

3.3 Satellite Brightness

If a casual observer didn't know artificial satellites existed, spotting one in the night sky might prove difficult to explain. Stars appear more or less stationary over the course of minutes, whereas meteorites slash bright arcs in less than a second. A LEO satellite, however, gradually appears out of nothingness. It may pulsate, flash, or have a barely perceptible tint of color. It takes minutes to move methodically across the sky in a perfect arc, then disappears as quietly as it came. Predictably determining when, where, and with what intensity such events occur is a source of constant challenge for satellite observers. This section describes how contemporary satellite observers evaluate and predict viewing opportunities.

Within contemporary satellite observing circles, three individuals are widely associated with satellite brightness predictions: McCants, Molczan, and Matson. For many years now, their contributions continue to greatly aid the efforts of semi-professional satellite trackers and now their names permeate this pastime's vernacular. Others deserve credit as well: there is no intentional slight by failing to include them here. The composite method described in this section incorporates multiple contributions: it is more than sufficient to meet this project's goals.[5]

To predict satellite brightness on any given overflight, this project uses a formula Robert Matson published (and often explained) online for the benefit of the satellite tracking community [*Matson*, 2008, 2001]. It is presented in its final form in Equation 3.16 below, but some additional explanation is helpful. For now, consider this generic logarithmic equation which describes an object's apparent magnitude (M_{app}) as a function of target distance, orientation, and an *intrinsic magnitude*. A satellite's intrinsic magnitude is conceptually identical to a star's absolute magnitude.

$$M_{app} = Intrinsic\ Magnitude + Distance\ Correction + Orientation\ Correction \quad (3.10)$$

---

[5]Higher-fidelity Iridium flare modeling is discussed in [*SeeSat-L User Group*, 2007]. In [*Henize et al.*, 1994], observed magnitudes are compared to satellite Radar Cross Section (RCS) data. For information on the optical properties of common spacecraft materials, consult [*Culp and Gravseth*, 1996]. Finally, [*Kervin et al.*] provides an overview of current government-funded research in optical tracking.

Generally speaking, a ground observer won't have an estimate of satellite attitude. Therefore, orientation corrections can only be a function of Sun-satellite-observer geometry. For this reason, orientation corrections are often calculated assuming satellites are Lambertian-scattering spheres. In this case, intensities of reflected sunlight vary only with changes in *phase angle*, η_{phase}:

$$\eta_{phase} = \cos^{-1} \left(\frac{\vec{r}_{LOS} \cdot (\vec{r}_{Sun} - \vec{r}_{sat})}{|\vec{r}_{LOS}| \, |(\vec{r}_{Sun} - \vec{r}_{sat})|} \right) \tag{3.11}$$

Phase angle varies from $0° \leq \eta_{phase} \leq 180°$. When $\eta_{phase} = 180°$, the object is directly between the observer and the Sun. Conversely, when $\eta_{phase} = 0°$, the object is fully illuminated (assuming the Earth wasn't blocking all the sunlight, of course). A right phase angle ($\eta_{phase} = 90°$) indicates a perpendicular light path between body and observer, exactly the same conditions under which a half-moon appears.

Understanding phase angle is critical, because two major intrinsic brightness catalogs are in common use; each relies on a different reference phase angle. Accordingly, different formulations of orientation corrections must be applied. They are dubbed the *McCants* and *Molczan* Methods, after their creators and the catalogs that use their respective assumptions.

Michael McCants' catalog of intrinsic brightness is in use since the 1960's. It assumes a full-phase reference angle ($\eta_{ref} = 0°$) and predicts the *brightest* magnitude likely to be observed. Michael McCants explains he chose this system "because I do not want to be 'surprised' that the object is 'brighter than predicted'"[*McCants*, 2008b]. Intrinsic magnitudes in the McCants catalog are identified using $M_{0°}$.

Alternatively, Ted Molczan selected a half-phase ($\eta_{ref} = 90°$) definition for his satellite catalog. It seeks to predict the likely *average* magnitude of an observed satellite. Many brightness values in this catalog are based on size and shape estimates, whereas others are observationally-derived: the catalog annotates which method was used for each satellite [*SeeSat-L User Group*, Undated]. This catalog is currently in the care of Michael McCants [*McCants*, 2008c]. Intrinsic brightness values published at *Heavens*

Above also use the Molczan Method [*Peat*, 2008]. Intrinsic magnitudes recorded using the Molczan Method are identified using $M_{90°}$.

Naturally, there is some debate regarding the merits of each system. Robert Matson suggests the Molczan method is worthy for four reasons, paraphrased here [*Matson*, 2008]:

- Because $\eta_{ref} = 90°$ is in the middle of the complete phase angle range, maximum extrapolation is only 90°. Extrapolation using the McCants method can reach as high as 160°.

- For most typical observations, $70° \leq \eta_{phase} \leq 130°$, so matching predictions near these angles will produce better results.

- Should a LEO satellite actually be observed near a full-phase angle of $\eta_{phase} = 0°$, atmospheric refraction and a lack of visible reference stars will complicate comparisons.

- A true full-phase measurement is impossible because the satellite will be in eclipse. If it could occur, there may be significant boosts in brightness due to direct reflections such as those from solar arrays.

To further complicate matters, there is an *approximate* conversion between the two systems, but Michael McCants' own disclaimers should be consulted before proceeding [*McCants*, 2008b]:

$$M_{0°} = M_{90°} - 1.5 \tag{3.12}$$

Whether half-phase or full-phase definitions are employed, a suitable orientation correction that is only a function of η_{phase} is still required. Robert Matson uses the term *phase factor* to describe just such a function assuming a solar-reflecting, Lambertian sphere [*Matson*, 2008, 2001]. This *phase factor* term is found within square brackets in Equation 3.13, where it identifies the scalar multiple increase or decrease in brightness with respect to $\eta_{ref} = 90°$, i.e. the Molczan Method. By encapsulating it in the common logarithm conversion explained in Equation 2.1, it now directly computes the expected

apparent magnitude of the satellite.[6]

$$Orientation\ Correction_{90°} = -2.5\log_{10}\left[\sin\left(\eta_{phase}\right) + \left(\pi - \frac{\pi\eta_{phase}}{180°}\right)\cos(\eta_{phase})\right] \quad (3.13)$$

Take note that at $\eta_{phase} = \eta_{ref} = 90°$, this term equals zero. Its maximum contribution occurs when $\eta_{phase} = 0°$, at which an object's apparent magnitude would decrease (become brighter) by ≈ 1.24 due to orientation alone.

If the origin of Equation 3.13 is unclear, a similar result will be re-derived for a full-phase McCants definition. It starts with the equation for the intensity of light scattered by a Lambertian sphere by a distant light source.[7] Irradiance, reflectance, and geometric constants are lumped, since they will soon be canceled in a ratio calculation (noting irradiance is identical regardless of the sphere's orientation, provided it is fully lit). The angle η, at this point, refers to any arbitrary phase angle [*Spiro and Schlessinger*, 1989]:

$$I = constants\left[\sin\left(\eta\right) + \left(\pi - \frac{\pi\eta}{180°}\right)\cos(\eta)\right]$$

The ratio of these two intensities, one arbitrary and one with $\eta_{ref} = 0°$, becomes:

$$\frac{I}{I_{ref,0°}} = \frac{constants\left[\sin\left(\eta\right) + \left(\pi - \frac{\pi\eta}{180°}\right)\cos(\eta)\right]}{constants\left[\sin\left(0°\right) + \left(\pi - \frac{\pi\times0°}{180°}\right)\cos(0°)\right]} = \frac{\sin\left(\eta\right) + \left(\pi - \frac{\pi\eta}{180°}\right)\cos(\eta)}{\pi}$$

Then, after Equation 3.13, the orientation correction for a McCant definition may be expressed.

$$Orientation\ Correction_{0°} = -2.5\log_{10}\left\{\frac{1}{\pi}\left[\sin\left(\eta_{phase}\right) + \left(\pi - \frac{\pi\eta_{phase}}{180°}\right)\cos(\eta_{phase})\right]\right\}$$
$$(3.14)$$

Now, this term has zero contribution when $\eta_{phase} = \eta_{ref} = 0°$. As η_{phase} increases, magnitude can only diminish as expected.

---

[6]Any angles within trigonometric functions are assumed to be calculated in degrees, to keep consistency with the remainder of the paper (the original source assumes angles in radians). Scalar factors ranging from 0 to π are still necessary due to the nature of the phenomena: π has nothing to do with radians in this case.

[7]Robert Matson adds that this same equation holds true for a Lambertian cylinder when viewed broadside. This models rocket bodies well, provided they are not viewed endwise.

Thankfully, both methods use the same reference distance of 1000 km. Changes in magnitude due to inverse square losses are expressed simply, provided $\vec{r}_{LOS}$ is always expressed in kilometers (km):

$$Distance\ Correction_{1000km} = 2.5\log_{10}\left[\left(\frac{|\vec{r}_{LOS}|}{1000km}\right)^2\right] = 5\log_{10}\left(|\vec{r}_{LOS}|\right) - 15 \quad (3.15)$$

By substituting the appropriate corrections into Equation 3.10, a complete formula for predicting satellite brightness is produced. For half-phase Molczan intrinsic magnitudes, the following equation as provided by Robert Matson is used [*Matson*, 2001]:

$$M_{app} = M_{90°} + 5\log\left(|\vec{r}_{LOS}|\right) - 15 - 2.5\log\left[\sin\left(\eta_{phase}\right) + \left(\pi - \frac{\pi\eta_{phase}}{180°}\right)\cos(\eta_{phase})\right]$$
$$(3.16)$$

If using full-phase McCants measurements the last term in Equation 3.16 should be substituted with the one found in Equation 3.14, and $M_{0°}$ used in place of $M_{90°}$. This method appears valid because it reproduces results from McCants' *Quicksat* program almost identically, given the same inputs.

The McCants method was primarily employed throughout this project in hopes of finding only the brightest likely targets. If intrinsic brightnesses from the McCants catalog were unavailable for a given object, values from either the Molczan or *Heavens Above* catalogs were converted using Equation 3.12, then processed in the exact same manner as original McCants values. Although this project did not quantitatively measure observed satellite brightness, this approach generally proved effective.

3.4   Targeting in the Local Horizon Frame

After extensive calculations, a short list of potentially fruitful opportunities is available. Chances are, the previous section's calculations disqualified a great number of objects. If our observing sensor (or vision) offered horizon-to-horizon coverage, additional information would be unnecessary. Unfortunately it does not, so the following question needs an answer: where and when shall we point our telescope?

If previously-mentioned parameters are available, this step is trivial. It requires the satellite's position vector $\vec{r}_{sat}$ and a 3×3 transformation matrix, $[C_{SEZ,ECI}]$, from Transformation 14 in [$Escobal$, 1965]. The matrix $[C_{SEZ,ECI}]$ is a function of θ_{site}, and ϕ. The SEZ-referenced vector is found using:

$$\vec{r}_{sat,SEZ} = [C_{SEZ,ECI}]\, \vec{r}_{sat,ECI}$$

$$\begin{Bmatrix} S_{sat} \\ E_{sat} \\ Z_{sat} \end{Bmatrix} = \begin{bmatrix} S_x & S_y & S_z \\ E_x & E_y & E_z \\ Z_x & Z_y & Z_z \end{bmatrix} \begin{Bmatrix} X_{sat} \\ Y_{sat} \\ Z_{sat} \end{Bmatrix} \tag{3.17}$$

The magnitude of the horizon vector, $|\vec{r}_{sat,SEZ}|$, is the *slant range* to the satellite. The satellite's compass azimuth A and elevation above the horizon h may be determined from $\vec{r}_{sat,SEZ}$ using any quadrant-checking conversion from cartesian to spherical coordinates. Venerable satellite tracking programs, such as *Quicksat* or *Heavens Above*, perform some variation of the calculations presented thus far to produce a tabular output of targets, times, azimuths, and elevations of interest for upcoming sorties[$McCants$, 2008a; *Peat*, 2008]. Armed with this data, the observer can head out with reasonable certainty of finding a satellite.

3.5 *Integrated Tracking Software*

Even if preparatory calculations indicate dozens of targets will appear during a given evening or morning, any number of obstacles stand in the way of successful data collection. Foremost of these is weather. Even if skies are partially clear, stray clouds can block out portions of the sky. Other times, a predicted target fails to appear at the designated time and place. Satellites can suddenly wink out of view if they happen to reenter the Earth's shadow or they fall into an unfavorable orientation. For casual observing, some of these phenomenon are quite entertaining. When collecting data, they are maddening.

To help overcome some of these obstacles, an interactive tracking package was developed using MATLAB$^{\circledR}$. At a glance, it gives the observer a comprehensive target list, expected overflight paths, a realtime video feed, and the ability to move the telescope and log data at will. If a pass isn't working out, a new target is sought on the fly. Should clouds block a portion of the sky, overflights in that region are avoided. This human-in-the-loop approach not only prevents wasted effort and null collects, but is certainly more entertaining than letting a computer pick every target.
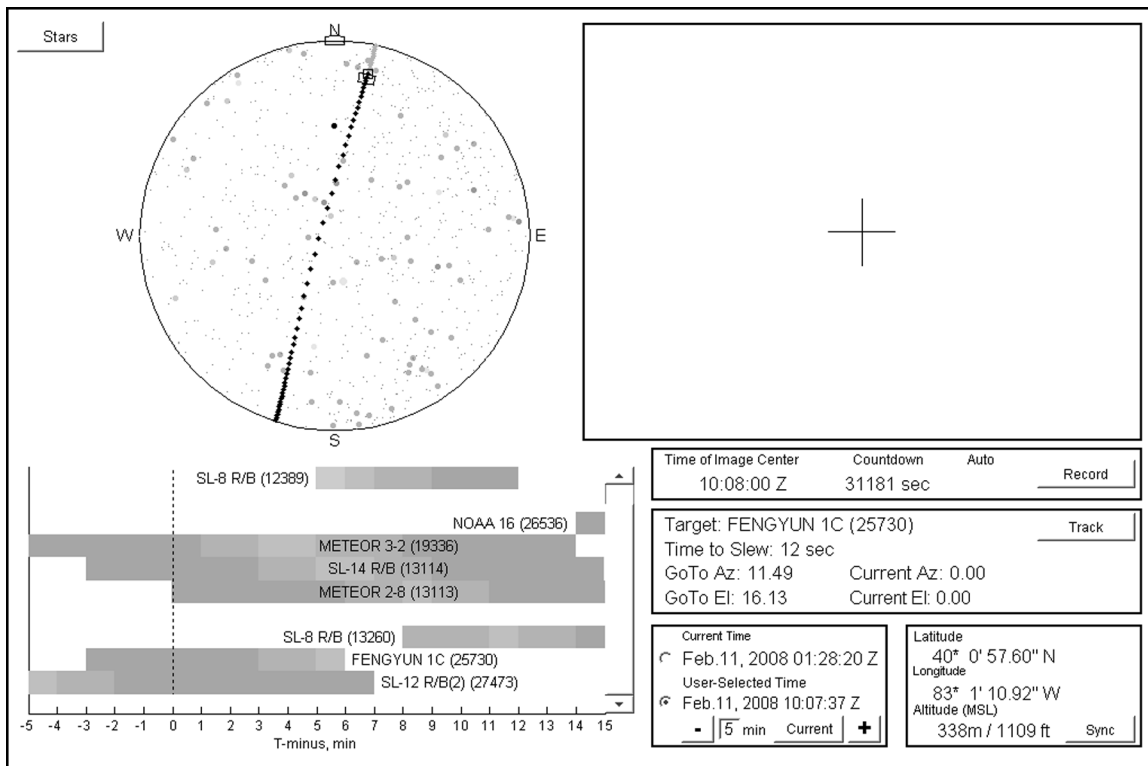
Figure 3.2:   Integrated Satellite Tracking Software

The goal of this interface is to allow the operator to execute any part of the tracking process simply and clearly. It makes every calculation except brightness predictions on demand (i.e. each time a satellite is targeted). Should new data become available during a session, such as an updated element set, it could be incorporated immediately. Other features include:

- Target Selection: A strip chart in the lower left features satellites of interest. It regularly updates, indicating what satellites are or will soon be overhead. To aid targeting selections, graduated bars indicate predicted brightness. Once a satellite is selected, a number of target-specific updates occur.

- Star Map: Predicted or current satellite overflights are displayed in the upper left, along with the telescope's current and targeted positions.[8]

---

[8]Astronomers may find this map "backwards," because it displays West on the left rather than right like a typical star chart. It is an indulgence of the terrestrially-minded.

- Video Display: The upper right portion features a realtime video feed. A count-down timer identifies the predicted time a satellite will cross the image center. Clicking on the record button logs the video feed and writes metadata to a computer file.

- Telescope Status: Just below the video display, a text readout shows the current and targeted pointing angles. A simple algorithm predicts the travel time to move between targets.

- Time and Position Data: Since the telescope is a mobile system, it is helpful to have a readout of where the system *thinks* it is. A GPS synchronization feature ensures the personal computer and telescope share navigational references.

This chapter developed a complete method for identifying bright satellites and tracking them. It is wholly reliant on published orbital element sets, accurate navigational data, and either observational or theoretically-determined brightness data. It is also an open-loop process that requires a human operator. In the next chapter, many of the transformations presented here will be reversed to produce inertial measurements. This moves us one step closer to develop our own orbit estimates, which in theory could eliminate complete reliance on only the NORAD catalog in future tracking efforts.

IV. Measuring Satellite Orbits

I̲F weather, equipment, and a user's basic competence combine to produce direct observations of satellite orbits, a key challenge emerges: how will grainy photographs or videos of streaking satellites become accurate inertial observations? Figure 4.1 shows the necessary elements required to convert collected metadata and videos into the inertial data necessary to perform initial orbit determinations.
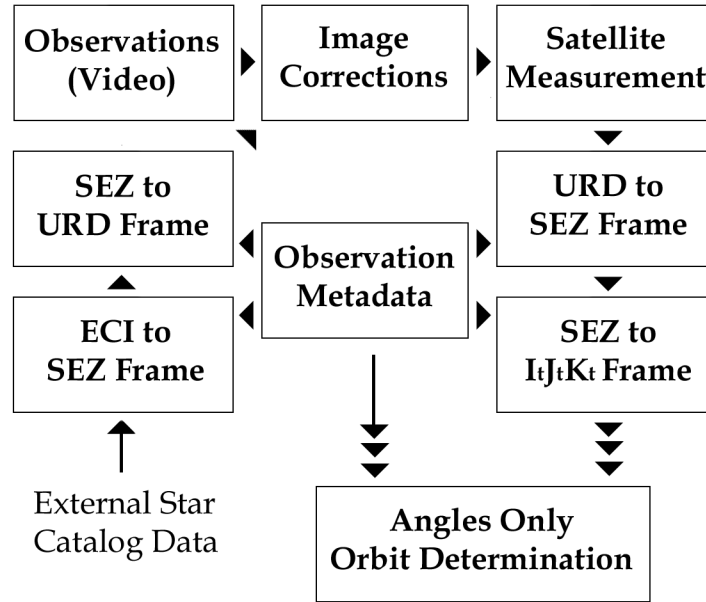
Figure 4.1:   Steps to Produce Inertial Measurements

Given the tools in Chapter III, nearly anyone could go out at night, look at a predicted location, then find and follow the tiny dot across the sky. If they were asked to describe when and where they saw it, however, it is unlikely they could produce useful measurements unless they were specially prepared for the task [*SeeSat-L User Group*, 1998]. The camera and telescope used in this project aid greatly the measurement process, because many key parameters are automatically logged. This section describes how measurements are made in the camera's reference frame, corrected with reference stars where available, and then converted to inertial measurements.

4.1   Establishing a Sensor Frame of Reference

The camera used in this project is mounted co-axially with the telescope, and the telescope is az-el mounted. Therefore, the Up-Right-Downrange (URD) reference frame is introduced, which allows video measurements to be converted back to the SEZ frame. It is a simple two-axis rotation that requires knowledge of the sensor's azimuth and elevation in the SEZ frame, (this information is provided by the telescope's computer when logging data).[1]
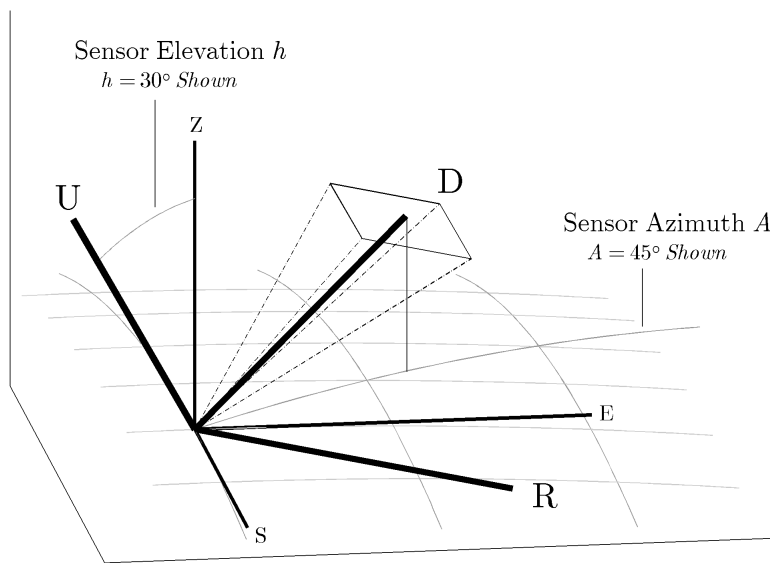
Figure 4.2:   Up-Right-Downrange (URD) Sensor Reference Frame

---

[1]The World War II anti-aircraft gun is a good analogy here: the camera is like the gunner always peering through the sight. From this point of view, a target is either up, down, left, or right of the barrel.

As evidenced by Figure 4.2, the sensor frame's horizontal axis R always remains parallel to the horizon (i.e. it is always in the S-E plane). The U axis points towards the top of the image plane (or "up" as viewed on a screen). The third orthogonal axis D lies exactly in the image center, extending downrange of the telescope (colloquially known as a boresight).

With this frame established, any unit vector in the SEZ frame is readily transformed to the image frame:

$$
\begin{Bmatrix} U \\ R \\ D \end{Bmatrix} = \begin{bmatrix} \cos(A)\cos(90^\circ - h) & -\sin(A)\cos(90^\circ - h) & \sin(90^\circ - h) \\ \sin(A) & \cos(A) & 0 \\ -\cos(A)\sin(90^\circ - h) & \sin(A)\sin(90^\circ - h) & \cos(90^\circ - h) \end{bmatrix} \begin{Bmatrix} S \\ E \\ Z \end{Bmatrix}
\tag{4.1}
$$
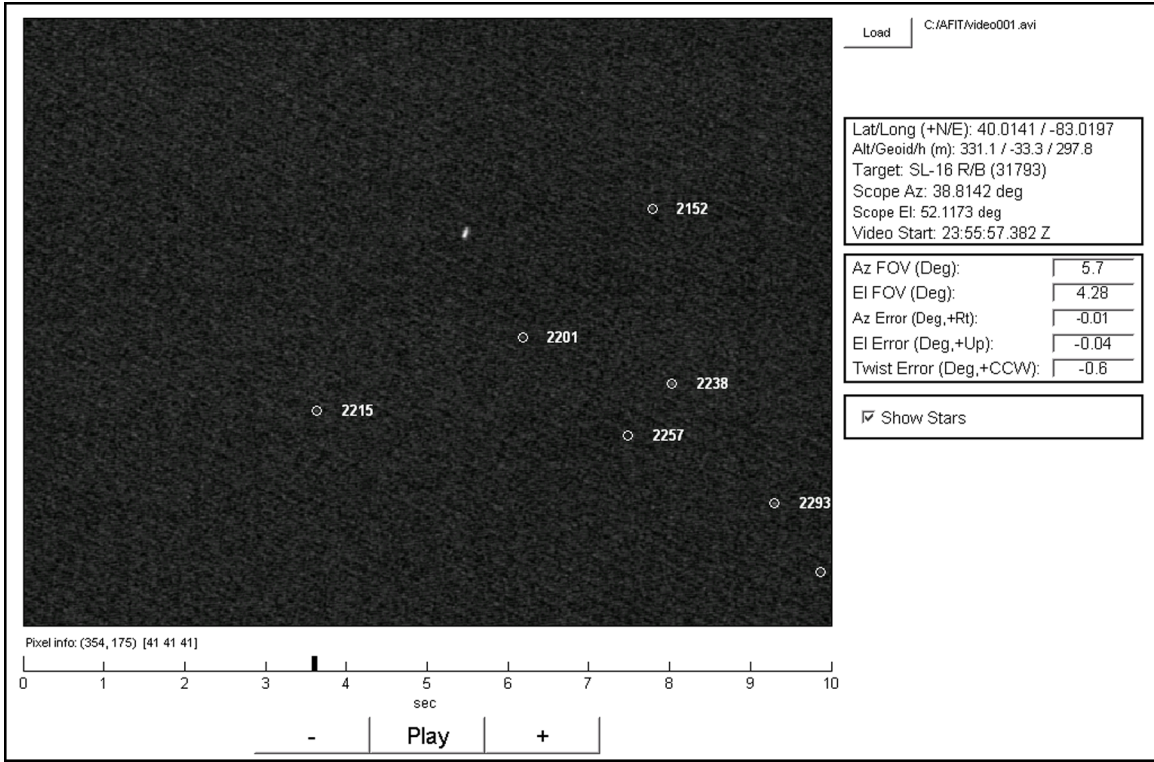
Figure 4.3:   Video Measurement Software

The SEZ-to-URD form is presented in Equation 4.1 because the first use of this frame is to project star locations onto collected videos. Using the methods described in Chapter III, the angular positions of celestial objects such as stars may be reduced

to pointing vectors in the URD frame for any given sensor attitude.[2] Then, a simple Cartesian to spherical conversion allows a determination of how many degrees up, down, left, or right of center an object *should* appear in any given image.[3] For example, say the frame transformation for a star's inertial pointing vector from the ECI (through SEZ) to the URD frame indicates a star is $1°$ up and to the right of the reported image center. This $1°$ figure is multiplied by the number of pixels per degree (a function of camera field of view and resolution) to plot the star's expected position directly on the video. Figure 4.3 shows the measurement software developed to accomplish this. Reference stars, with their associated identifiers, are scattered throughout the video frame. These predicted star locations now aid the satellite measurement process, which the next section will describe in greater detail.

4.2   Corrections in the Sensor Frame

It is unlikely any collected image perfectly agrees with its associated metadata, so a critical first step is correcting for misalignments. Using the software shown in Figure 4.3, projected stars may be lined up with those collected on the video. Figure 4.4 shows three common kinds of misalignments: azimuth (Δ_A), elevation (Δ_h), and camera twist (γ).

Currently, the correction process relies on a human operator to identify necessary corrections in the video measurement software in trial-and-error fashion. The user's goal is to make all recorded stars appear within their corresponding theoretically-determined projection (see Figure 5(b) for an example). Typically, the camera's twist γ is determined first: comparing projections to any video with more than three stars usually produces a reasonable estimate.[4] Then, the image is translated left or right (Δ_A), then up or down

---

[2]This project used formulas from [*Meeus*, 1998] to account for precession and nutation of the *inertial* axis, as well as proper motion and atmospheric refraction.

[3]Since pointing vectors have unit magnitude, the vector's length (often called ρ) is irrelevant.

[4]The twist angle γ, as determined from calibration videos, is used in other observations where only one star is visible. Twist errors are static throughout a single sortie.
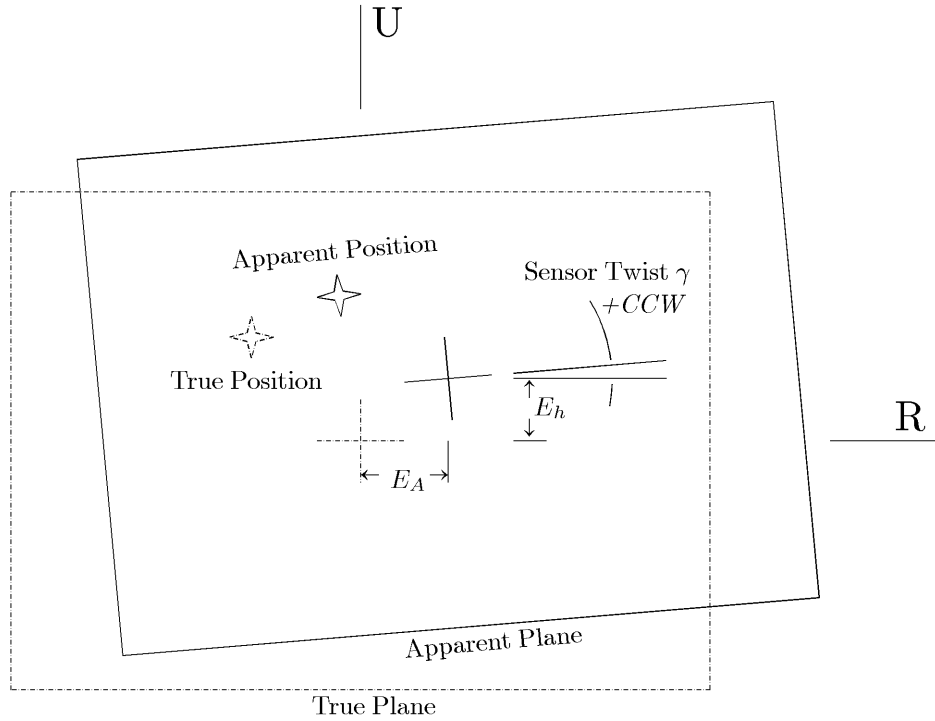
Figure 4.4:   Misalignments in the Sensor Plane

(Δ_h), until all visible stars and projections match. Although it is possible some alternate permutation of the selected corrections could produce a match, this seems unlikely.[5]

Once these steps are complete, a satellite streak is measured (see Figure 5(c)) to produce an uncorrected pointing vector in the uncorrected URD frame. Thanks to the star alignment process, most inaccuracies may now be remedied. First, any camera twist is canceled with a single-axis counter-rotation about the image center by the angle γ. Then, the azimuth and elevation reported in the metadata is modified by adding Δ_A and Δ_h. This produces a true apparent URD line-of-sight vector, which is then transformed to the SEZ frame using the inverse of Equation 4.1. Once in the SEZ frame, the effects of generic atmospheric refraction are subtracted to produce an airless azimuth and elevation measurement. Now, the user has the necessary information to produce a single line-of-

---

[5]Stars' positions are also updated frame-by-frame, allowing the user to verify they are drifting at the appropriate sidereal rate. In this sense, this process is three-dimensional astrometry: two dimensions are represented by the apparent star position on the image plane, and the third dimension is time.

sight vector, pending one final transformation. The next section describes this step in detail.

4.3 The Topcentric Reference Frame

Thankfully, there is only one more frame transformation standing between the satellite tracker and an orbit determination. Most angles only methods make use of the Topocentric Reference Frame $(I_t J_t K_t)$, referred to here as it is in [*Vallado and McClain*, 2007]. Simply explained, it is a reference frame that is always aligned with the ECI frame, but whose origin is coincident with the observing site. Transformation of SEZ to $I_t J_t K_t$ line-of-sight vectors is a function of θ_{site} from Equation 3.4 and site geodetic latitude ϕ.

$$
\left\{ \begin{array}{c} I_t \\ J_t \\ K_t \end{array} \right\} = \left[\begin{array}{ccc} \cos(\theta_{site})\cos(90° - \phi) & -\sin(\theta_{site}) & \cos(\theta_{site})sin(90° - \phi) \\ \sin(\theta_{site})\cos(90° - \phi) & \cos(\theta_{site}) & \sin(\theta_{site})\sin(90° - \phi) \\ -\sin(90° - \phi) & 0 & \cos(90° - \phi) \end{array} \right] \left\{ \begin{array}{c} S \\ E \\ Z \end{array} \right\}
\tag{4.2}
$$

Any of the measurements produced using the process described in Section 4.2 can be converted to topocentric line-of-sight vectors using Equation 4.2. Of these, the three vectors with widest angular separation are typically used to calculate orbits: they will be referred to as $\hat{\vec{l}}_{first}$, $\hat{\vec{l}}_{mid}$, and $\hat{\vec{l}}_{last}$, respectively. Chapter V explains that although there are some challenges to computing orbits with such measurements, it is possible to get useful predictions given the right conditions.

V. Results and Discussion

THIS project began with a simple goal: use a commercial telescope to track satellites and determine their orbits. Within the span of even a few sorties, the fundamental capabilities and limitations of a system like this one appear:

- A single-site telescope, under the right conditions, can produce sensible initial orbit estimates. Geometry dominates solution quality, however. This geometry is outside the engineer's control, so ill effects must be understood and tolerated.

- This prototype system is accurate enough to produce Cartesian state vectors (and therefore classic orbit elements) given appropriate observing geometry.

- Investing in sensor precision does not necessarily yield matching dividends in a telescope's ability to determine initial LEO orbits. Since many LEO observations may suffer from singular behavior, using many lower-precision sensors may be better than using a few precise ones.

This chapter elaborates on these points, first by explaining observational limitations in the angles-only method. Section 5.1 explains this using case studies from collected data. Then, Section 5.2 relates the prototype accuracy of this system and demonstrates an initial orbit calculation. Finally, Section 5.4 shows how well a case study orbit propagates to aid future tracking network design.

5.1 Angles-Only Data and the Great Circle Deviation

It is well-established that using only pointing vectors to determine satellite orbits is a quirky prospect. David Vallado assesses,

> Gauss's method using angles-only data receives mixed reviews from the astrodynamic community. The opinions range from little concern because the method works best for interplanetary studies, to feeling that it's not very accurate for satellite-orbit determination, to reverence for the achievement realized at a time when data was limited. [*Vallado and McClain*, 2007]

One key phenomenon that leads to enormous consternation is introduced here, using the adopted term *great circle deviation*.[1] Its effects certainly contribute to the ambivalent

---

[1]A *great circle* is the shortest arc connecting two points on a sphere. Aircraft and ships use great circle navigation to travel the shortest possible distance between destinations.

attitudes Vallado notes above. It is a counterintuitive concept for most engineers, because this phenomenon dictates that *regardless of instrument accuracy, accurate results (or any results at all) may not be attainable.* Based on data collected during this project, however, it is the dominant parameter affecting success or failure of any attempted orbit calculation from a single ground observer. Therefore, its effects must be explored.

In *Fundamentals of Astrodynamics*, the authors Bate, Mueller, and White reference work by Moulton; he found that an angles-only solution (in this case the Laplacian) fails when "the three observations lie along the arc of a great circle as viewed from the observation site at [the middle time]." In an inertial sense, this occurs when the observing site is in the orbit plane during the observation [*Bate et al.*, 1971]. Consequentially,

- Topocentric observations that form a great circle will fail to produce orbit solutions.

- This condition is unstable: minute errors near this point cause huge deviations in results. Solutions derived from near-great-circle observations are suspect.

- Deviation from the great circle observation is proportional to the site distance from the orbit plane.

Simply put, a telescope must have the ability to look "down" on the orbit in order to observe its arc. Imagine placing dozens of ants on a table and watching them wander around on a red-and-white checkered tablecloth. It's easy to trace the path of any single ant, as well as determining if it's on a red or white square. Now, attempt the same thing with your eye at the table's edge: it's hard to tell the difference between large, distant ants moving quickly or close, small ants moving slowly. Placing them on a red or white square becomes nearly impossible.

This same problem often occurs when observing LEO satellites with a telescope. Oftentimes, the ground site is at or near the orbit plane and therefore can't see the orbit's arc. As points of light, the track could be a small, close ant or a distant large one. The orbit plane is clear (we know we're looking at the table's edge), but it's impossible to determine the satellite's range, or in other words how many red and white squares are between us and the ant.

Keeping these phenomena in mind, consider the following case study: the apparent path of two distinct satellites are carefully measured by a ground observer. An orbit determination for each is eagerly computed, and the results compared to those predicted by the SGP4 algorithm derived from NORAD catalog data.[2] For this case study, results from south-to-north overflights of an SL-8 rocket body (20433) and Cosmos 1980 (19649) are presented. Table 5.1 lists the bulk deviations from the expected SGP4 predictions. The angles between the observed and SGP4-predicted topocentric line-of-sight measurements $\Delta \hat{\vec{l}}_{first}$, $\Delta \hat{\vec{l}}_{mid}$, and $\Delta \hat{\vec{l}}_{last}$ are provided as an indication of overall angular accuracy of the measurement: note the similar values. The net error of the calculated Gauss/Gibbs solution is computed by subtracting its computed position and velocity vectors from their corresponding SGP4-predicted values. The magnitude of these errors are listed as E_r and E_v, respectively.

Table 5.1:   Observation and Orbit Determination Errors for SL-8 and Cosmos 1980 Overflights

	SEZ Arc	$\Delta \hat{\vec{l}}_{first}$	$\Delta \hat{\vec{l}}_{mid}$	$\Delta \hat{\vec{l}}_{last}$	E_r [km]	E_v [m/sec]
SL-8 Rocket Body	62°	0.127°	0.029°	0.136°	93.3	-892
Cosmos 1980	67°	0.157°	0.018°	0.161°	0.63	14.82

Why is it that one calculation produced useful results, but the other was significantly fouled? For a prototype system, initial guesses would involve timing or pointing inaccuracies, miscalculations of reference points, optical misalignments, and any other number of mundane possibilities. In this case or any other, attempting to correct time, azimuth, and elevation data or find clear trends between them and solution accuracy usually proves fruitless. A clear answer emerges only after examining the collection geometry, presented in Figure 5.1.

---

[2]Although the accuracy of NORAD SGP4 predictions is considered dubious on some scales, for this example they are sufficient.
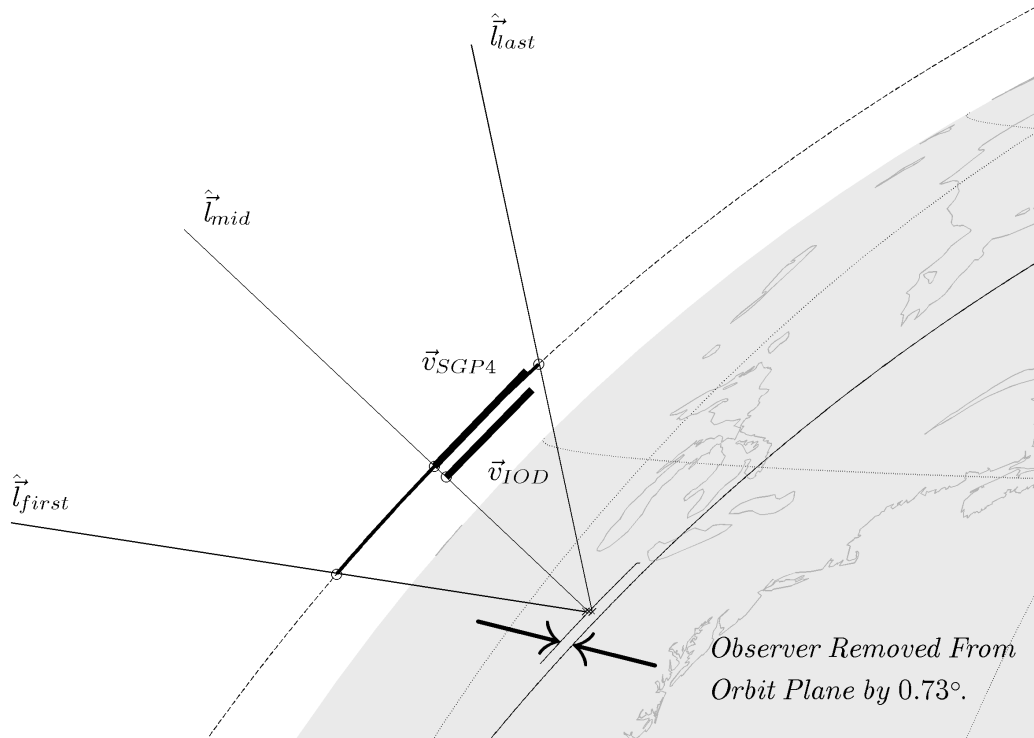
(a) Overflight of SL-8 Rocket Body (20433) on 16 January 2008
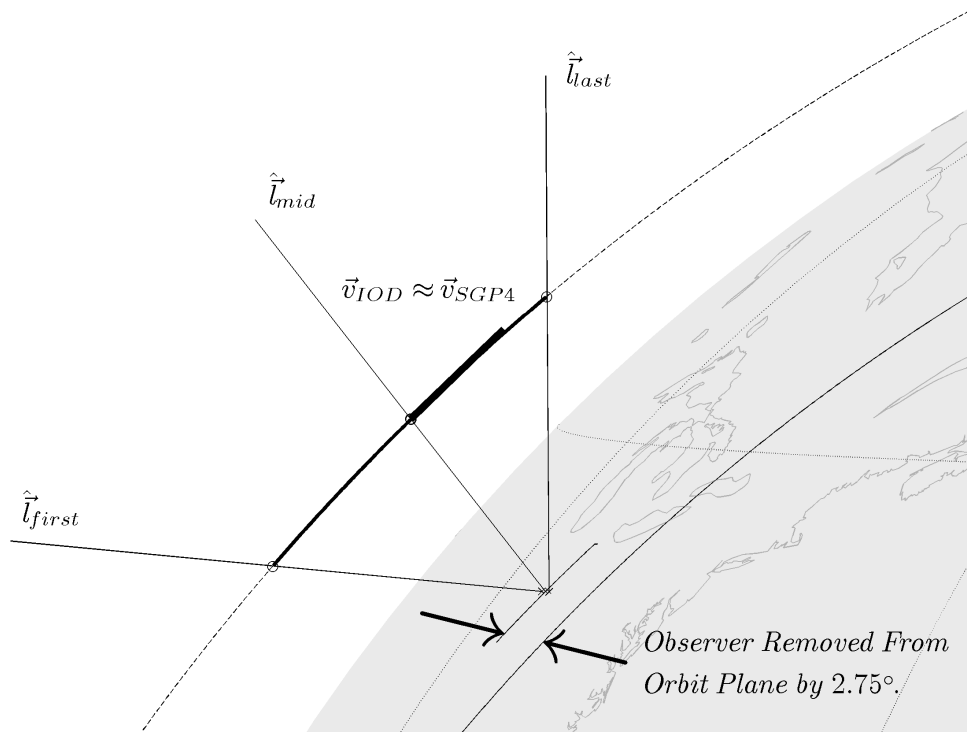
(b) Overflight of Cosmos 1980 on 3 February 2008

Figure 5.1:   Two Similar Satellite Overflights

41

After inspecting these orientations, it is readily apparent that the SL-8 track occurred when the angle between the observing site and the rocket body's orbit plane was a scant 0.73°. This places it very near the table's edge. The Cosmos 1980 track, on the other hand, enjoyed over three and a half times more separation at 2.73°. The calculated results are no longer so perplexing.

One problem remains, however. Identifying these very telling planar orientations requires solid knowledge of the target's orbit. Since the goal is to *determine* the orbit given no other information, some other method of identifying near-singular conditions is required. Moulton's original description of the singular great circle condition proves useful in this endeavor.

Measurements are reduced to produce three topocentric pointing vectors ($\hat{\vec{l}}_{first}$, $\hat{\vec{l}}_{mid}$, and $\hat{\vec{l}}_{last}$). Using only these measurements, a measure of merit the author calls great circle deviation (ζ_{GC}) is proposed; it is computed in the following manner:

- Find a unit vector perpendicular to the "great circle" plane that passes through both $\hat{\vec{l}}_{first}$ and $\hat{\vec{l}}_{last}$:[3]

$$\hat{\vec{l}}_{GC} = \frac{\hat{\vec{l}}_{last} \times \hat{\vec{l}}_{first}}{\left| \hat{\vec{l}}_{last} \times \hat{\vec{l}}_{first} \right|}$$

- Find the projection of the middle topocentric observation $\hat{\vec{l}}_{mid}$ onto $\hat{\vec{l}}_{GC}$, $\vec{a}_{mid}$:

$$\vec{a}_{mid} = (\hat{\vec{l}}_{mid} \cdot \hat{\vec{l}}_{GC})\hat{\vec{l}}_{GC}$$

- Find the projection of $\hat{\vec{l}}_{mid}$ onto the great circle plane, $\vec{b}_{mid}$:

$$\vec{b}_{mid} = \hat{\vec{l}}_{mid} - \vec{a}_{mid}$$

---

[3]Formally, a great circle is the circle formed by the intersection of a sphere and a plane passing directly through its center. Moulton referenced vectors only to the middle observation time, so this analysis does as well. The vectors $\hat{\vec{l}}_{first}$ and $\hat{\vec{l}}_{last}$, when referenced to the site's position at the middle observation time, form a great circle intersection with a unit sphere.

- Compute the angle between the middle observation and its projection onto the great circle plane:

$$\zeta_{GC} = \cos^{-1}\left(\frac{\vec{a}_{mid} \cdot \vec{b}_{mid}}{|\vec{a}_{mid}| \left|\vec{b}_{mid}\right|} \right) \tag{5.1}$$

Finally, it is possible to determine why some observations fail to produce useful initial state vectors and others do, even though the telescope's accuracy is constant. In the course of three sorties, hundreds of measurements were made on 14 distinct satellites.[4] Figure 5.2 shows comparative plots of initial position and velocity estimates from these observations ($\vec{r}_{IOD}$ and $\vec{v}_{IOD}$) versus ζ_{GC}. These observational results confirm theory, clearly identifying singular behavior as ζ_{GC} approaches zero. Since only a few observations resulted in high values of great circle deviation (they were exceptionally fortunate observations), their observed arcs are split up into sub-arcs, and those sub-arcs are individually analyzed. This not only fills out the plot, but highlights following: an observer must be outside the orbit plane to achieve high ζ_{GC} values, but the reverse is not true. A highly separated observer catching only a small arclength observation will produce measurements with low ζ_{GC} values, so successful initial orbit determination is unlikely. In the case of the highlighted Cosmos 1980 and SL-14 Rocket Body (18215) passes, results would be very poor if the full-length observation was not collected.

---

[4]See Appendix C for select observations of these satellites.
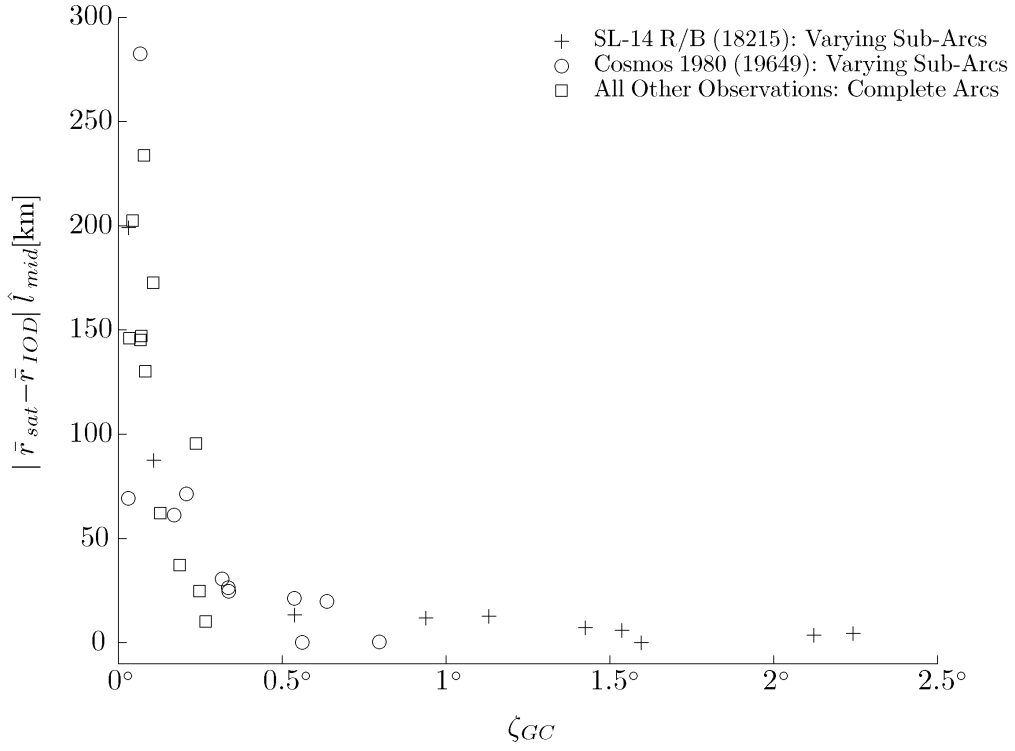
(a) Absolute Value of Position Errors in True Range Direction
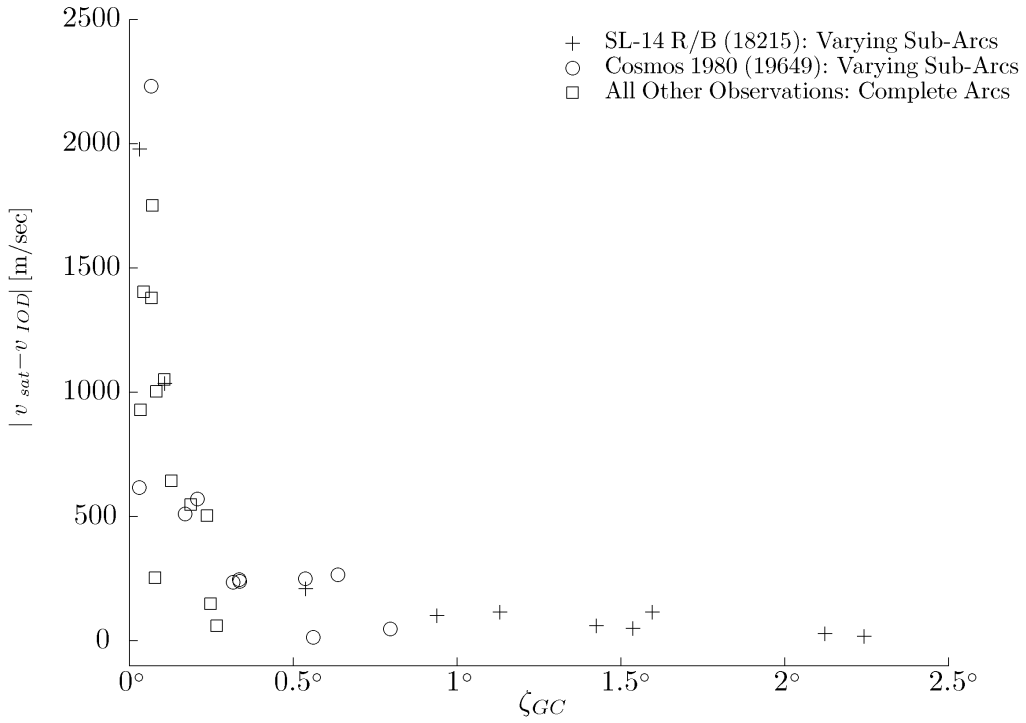
(b) Absolute Value of Net Orbital Velocity Errors

Figure 5.2:   Position and Velocity Errors vs. Great Circle Deviation

To explore the impact of arclength on ζ_{GC}, and add further support to the claims made here, theoretically-determined azimuth and elevation measurements computed as in Chapter III are used instead of collected ones in a Gauss/Gibbs angles only routine.[5] Again, using Cosmos 1980 and the SL-14 as a case study, ζ_{GC} is calculated as a function of the arclength of observation for the same scenarios already discussed. Figure 5.3 shows these results, which confirms ζ_{GC} is a function of both the arclength of observation and separation from the orbit plane at the middle observation. If it were a function of arclength only, the two lines would be coincident. Finally, it implies that the closer to the orbit plane an observer is, the greater the observation arclength must be to achieve the same ζ_{GC} value and associated confidence in the initial orbit determination.
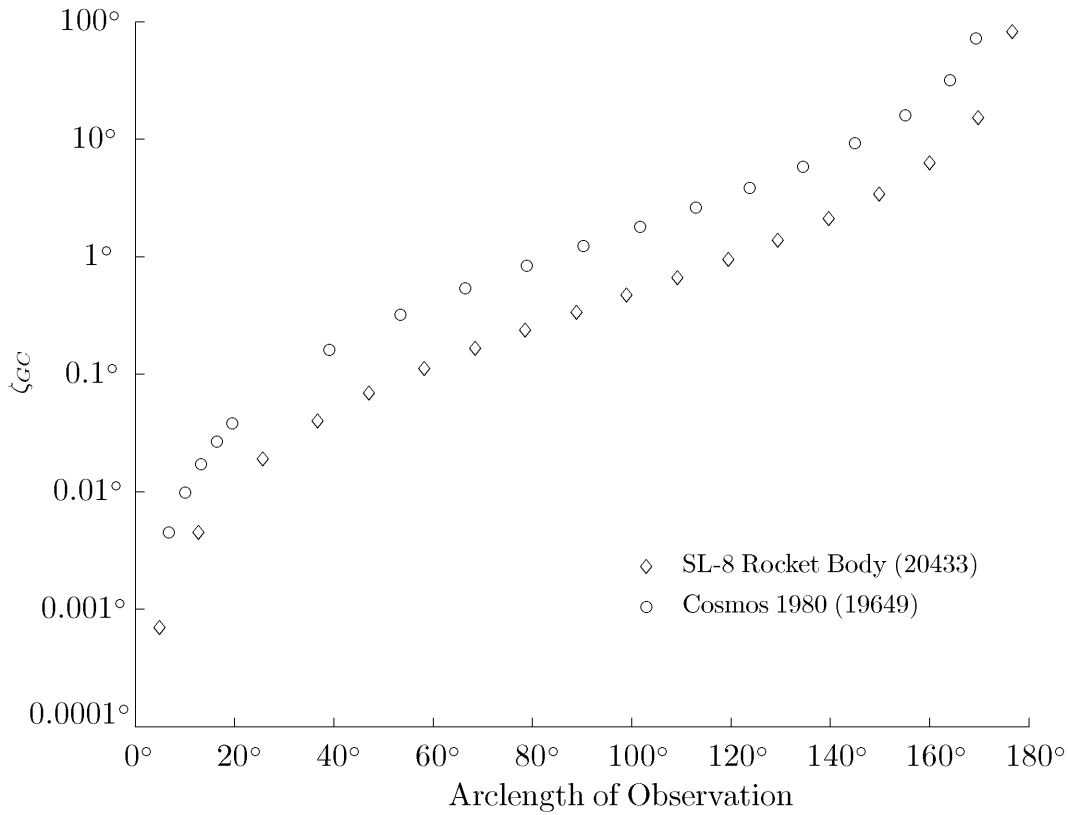
Figure 5.3: ζ_{GC} Versus Theoretical Arclength of Observation for SL-8 Rocket Body (20433) and Cosmos 1980 (19649)

---

[5]When compared to a line-of-sight vector computed directly from $\vec{r}_{sat}$ and $\vec{r}_{site}$, these "perfect" measurements produced a net angular difference of $0.0005 \pm 0.002°$. This is probably due to some necessary interpolations. This is about half the angular accuracy of a *Raven* system, but sufficiently close to true for this argument [*Thrall*, 2005].

The second purpose of the case study is to show that, even with very accurate measurements, the same basic phenomena are observed. Figure 5.4 shows absolute errors in range and velocity estimates for theoretical data, just as Figure 5.2 showed them for experimental data. The important item to note is the singular behavior near $\zeta_{GC} = 0°$, which confirms the experimentally-determined results. Future research may explain why, in these plots, accuracy gets much better shortly before it gets much worse. This effect is not observed in the experimental data to date.

Understanding the impact of great circle deviation on a telescope's ability to produce orbits is critical. It is a sobering proposition: both a million-dollar telescope and a fifty-dollar camera, sitting next to each other in the orbit plane of a target satellite, are both useless for determining state vectors by themselves. Granted, a more accurate instrument could produce better results at lower values of ζ_{GC}, but theory demands that dividends diminish exponentially regardless of the investment.

It should also be noted that this effect is greatest for short observations, which is the norm for optical LEO tracking. It is exacerbated by the fact that these objects are usually illuminated only when the observer is close to the orbital plane in the first place.[6] When tracking higher altitude targets, the Earth will rotate further through the target's orbital plane or be further separated from it in the first place (as with GEO satellites, unless the site is equatorial). This results in much higher ζ_{GC} values and fewer complications.

[6]Extremely low elevations correspond to high orbit plane separation. Except for the highest latitudes, a low elevation observation in an easterly or westerly direction would usually place the satellite behind the Earth's shadow (no reflected sunlight) or between the observer and the Sun (little or no reflected sunlight). Since many LEOs are in highly-inclined orbits, the only time these conditions are avoided is when passing at higher elevations, which means smaller orbit plane separation.
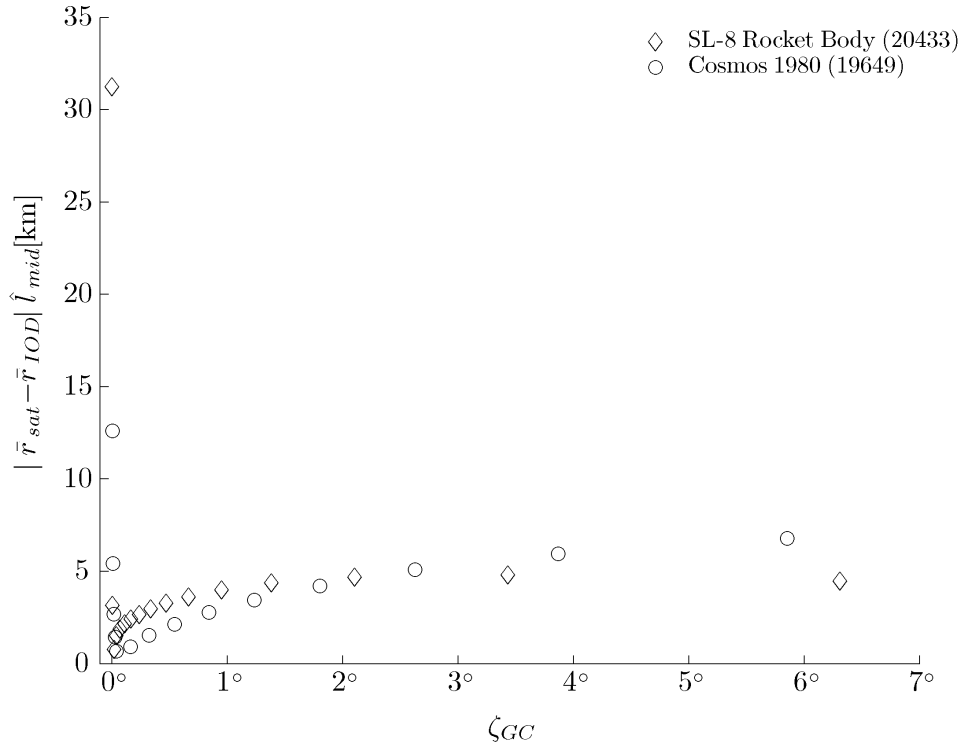
(a) Absolute Value of Position Errors in True Range Direction, Theoretical Data
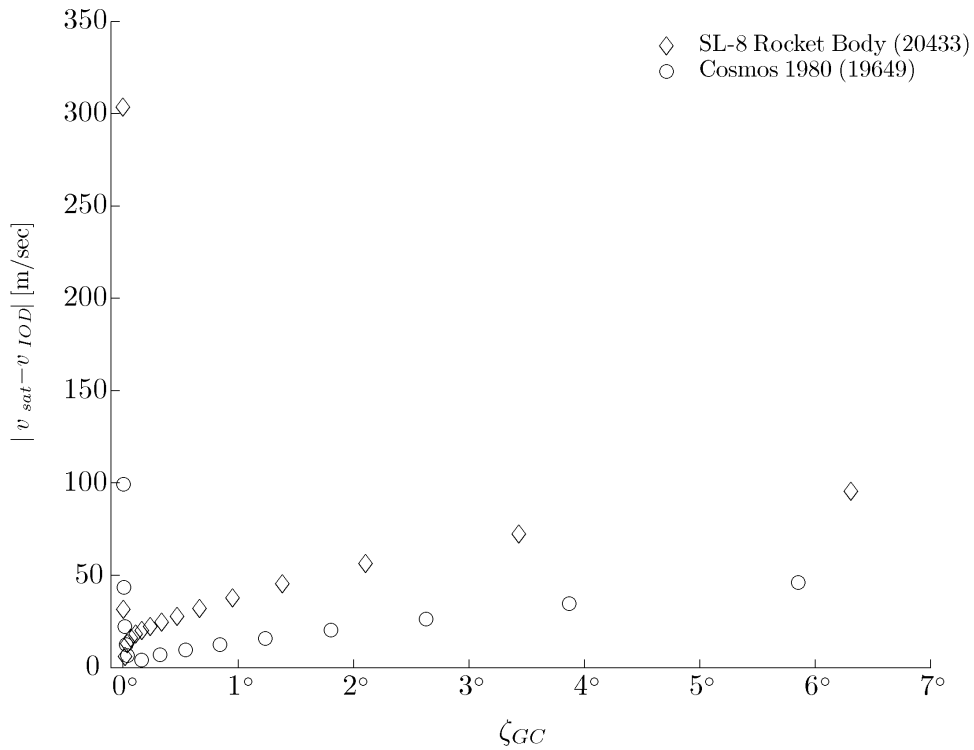
(b) Absolute Value of Net Orbital Velocity Errors, Theoretical Data

Figure 5.4:   Position and Velocity Errors vs. Great Circle Deviation, Theoretical Data

47

5.2   Prototype Accuracy and Precision

In the previous section, the impact of great circle deviation was emphasized to simplify the discussion of overall system accuracy. Figure 5.2 shows a sharp cutoff where great circle deviation is no longer the dominant source of error ($\approx 1°$ or greater based on experimental results). This cutoff threshold, and the accuracy of any results obtained beyond it, is now dominated by much more linear angular and temporal parameters.

As discussed in Chapter II, there are a few major sources of error in angles only computations: time, site location, and sensor azimuth and elevation. Accordingly, a telescope will have associated accuracy and precision for each. Accuracy is determined through calibration, whereas precision is dependent on measurement resolution. This section establishes these parameters for this prototype system. The most important parameters are azimuth and elevation precision and timing accuracy, which are summarized in Table 5.2.[7]

Table 5.2:   Angular and Timing Accuracy

Angular Accuracy (3σ):	$\pm 0.05°$
Timing Accuracy (3σ):	± 0.5 seconds

Both the timing and site location accuracy of this system is wholly dependent on the telescope's GPS receiver. Individual chips used in commercial telescopes vary, but the specific LX200GPS used in this project employs a Sony GXB5210. Due to the fact it reports time to the nearest second and position to the nearest second of latitude and longitude, it is assumed to be accurate to at least these values.[8] Once synchronized, timing precision is a function of the CPU clock, software, and the webcam's framerate output. Since negative effects of timing precision remain unobserved, it is considered to have negligible impact on computed results.

---

[7]For reference, the original Moonwatch teams first claimed to make angular measurements within $1°$ with one second timing. With practice, some groups claimed six arcminutes ($\approx 0.004°$) and 0.1 second accuracy [*Engle and Drummond*, 1965]. Contemporary telescopes in the *Raven* system achieve one arcsecond ($\approx 1 \times 10^{-5}$ degrees) accuracy [*Thrall*, 2005].

[8]Refer to [*Sony Corporation*, Undated] for chip specifications, and Appendix A for more on complications in using the onboard receiver.

Establishing angular measurement accuracy is accomplished through astrometric correction. Using techniques presented in Chapter III, inertial line-of-sight vectors for any visible stars are transformed into the URD plane. Then, each star's identifier and location is plotted directly on the video.[9] Figure 5.5 shows an example of a well-populated starfield, as well as details of a star and bright satellite as they appear on a typical video.
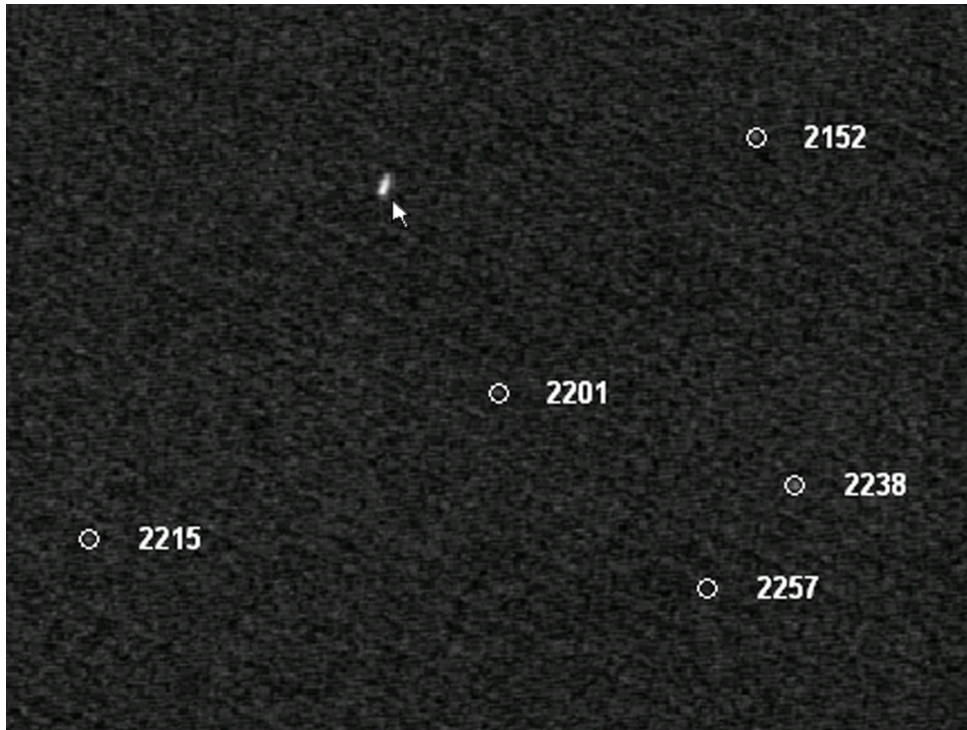
(a) Well-Populated Reference Starfield

(b) Star With Correlated Position
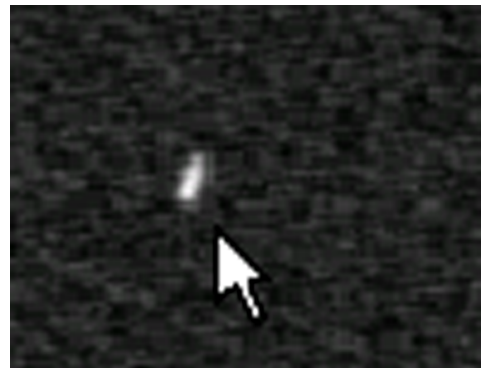
(c) Bright Satellite Image

Figure 5.5:   Examples of Video Measurement

---

[9]The Yale Bright Star catalog is used, which is available at [*Hoffleit and Warren*, 1991].

First and foremost, the angular accuracy of the inertial to URD transformations and their subsequent display is confirmed by the fact that, once minor corrections to reported azimuth, elevation, and twist are made, it is possible to align all reference stars with those on the video. Additional confirmation is made by computing arclengths with the software, then comparing results with standard formulas with the same purpose, such as those found in [*Meeus*, 1998]. This accuracy only applies when reference stars are visible, however.[10]

In its current configuration, each pixel spans approximately 0.009°, so it would be tempting to use that as a measure of system precision. There is naturally some error in placing reference stars as well as selecting the leading portion of a satellite streak, however. Since it is likely that any given user can click inside or very near the circle as shown in Figure 5(b) nearly all of the time, that span should serve as a suitable 3σ precision. An angle of 0.05° proves to be a suitable estimate based on the span of star images and empirical analysis.

5.3   Calculating an Initial Orbit Determination

Having established both the conditions under which initial orbit determination is possible and the expected accuracy of the system, it is possible to show that this system is capable of producing a useful state vector. As Section 5.1 noted, one observation produced a measurement with a much higher ζ_{GC} value than any other collected so far. This observation corresponds to an SL-14 Rocket Body (18215). If the claims presented so far are true, a calculated initial state vector should be relatively accurate. Figure 5.6 shows the observation geometry for this overflight.

Topocentric measurements in the $I_t J_t K_t$ frame are developed using methods from Chapter IV, and a Gauss/Gibbs angles-only routine from [*Vallado and McClain*, 2007] is used to determine the satellite's orbit. Results are computed in Monte-Carlo fashion: each observation's nominal time, azimuth, and elevation measurements are perturbed within the 3σ values found in Table 5.2. For each perturbation, new topocentric pointing

---

[10]If no reference stars are present, measurements must rely on mount accuracy. Due to minor problems as noted in Appendix A, only measurements with star references are currently included in this analysis.
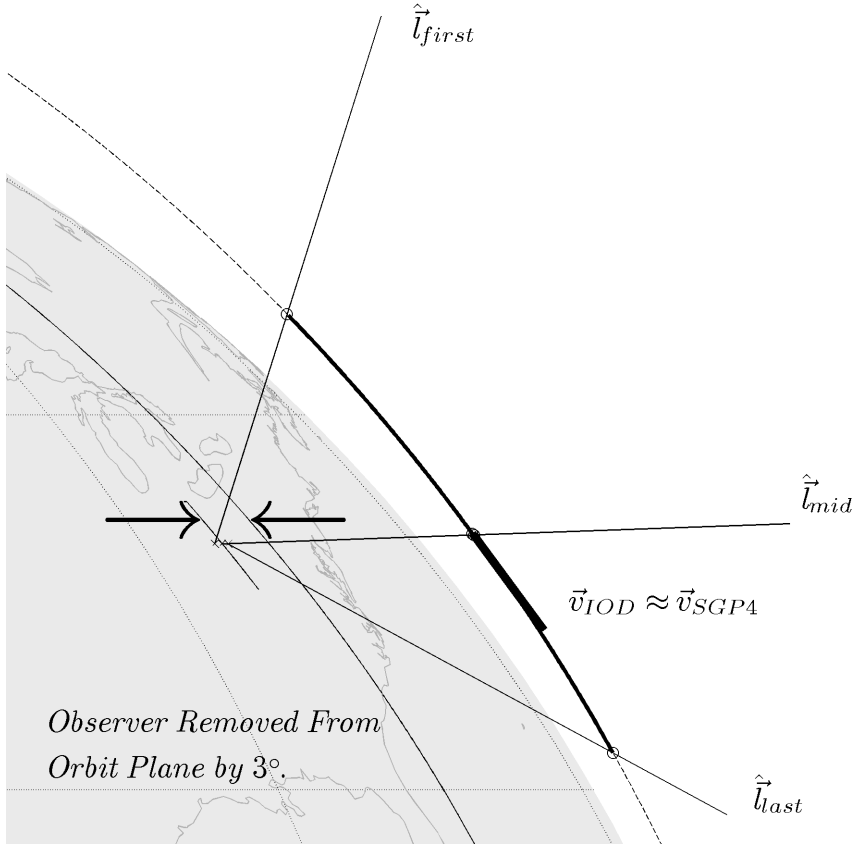
Figure 5.6:   Overflight of SL-14 Rocket Body (18215) on 3 February 2008

vectors $\hat{\vec{l}}_{first}$, $\hat{\vec{l}}_{mid}$, and $\hat{\vec{l}}_{last}$ are computed. For each set of three observations, a Cartesian position and velocity vector is generated: a mean solution with expected 3σ deviations was produced from these Cartesian vectors. Figure 5.7 shows a comparison between the computed and NORAD orbits. Table 5.3 compares state vector results to those extracted using the SGP4 propagator, followed by the classical orbital element sets in Table 5.3. When examining orbital elements, remember that large variations in ω and M are expected for nearly-circular orbits. Summing the two produces the Argument of Latitude (μ): this parameter confirms the orbits are similar [*Bate et al.*, 1971].

(a) Angles Only Orbit, Cross-Plane

(b) SGP4 Orbit, Cross-Plane
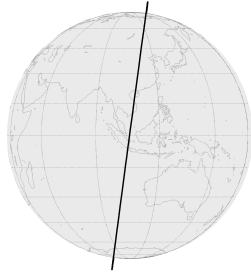
(c) Angles Only Orbit at Ω, Equator
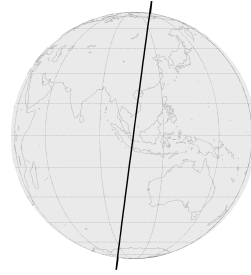
(d) SGP4 Orbit at Ω, Equator

Figure 5.7:   Graphic Comparison of Angles Only vs. SGP4 Orbits

Table 5.3:   Gauss/Gibbs Initial Orbit Determination Results for SL-14 Rocket Body (18215), Epoch 3 Feb 08 00:28:32.1Z

	r_x	r_y	r_z [km]
Gauss/Gibbs Angles Only	2784.8 ± 3.66	4948.4 ± 10.2	4081.5 ± 2.52
NORAD/SGP4	2785.6	4949.9	4086.6
	v_x	v_y	v_z [m/sec]
Gauss/Gibbs Angles Only	1067.0 ± 39.8	4403.5 ± 36.2	-6047.6 ± 51.4
NORAD/SGP4	1076.0	4384.3	-6052.0

Table 5.4:   Orbital Element Sets for SL-14 Rocket Body

	Angles Only	NORAD/SGP4
Inclination (i)	82.406°	82.510°
Right Ascension of the Ascending Node (Ω)	246.13°	246.06°
Argument of Periapsis (ω)	104.16°	184.73°
Eccentricity (e)	0.00232	0.000955
Semimajor Axis (a) [km]	7005.41	7002.30
Mean Anomaly at Epoch (M)	39.60°	319.26°
Argument of Latitude (μ)	143.76°	143.99°

5.4 Impact on Tracking Network Design

Results shown here are promising. With only a single observation, a relatively accurate state vector is determined. This section describes how, hypothetically, a system like this one could contribute to a larger tracking network, or perhaps be duplicated to compose one of its own. Although further assessments are left to future research, this section examines how effectively the case study orbit *would* have worked if it put to better use.

Any initial satellite orbit estimate, even a good one, will quickly lose utility. To keep discussions straightforward, it is common to talk about an orbit's in-track and cross-track accuracy. Of these, cross-track accuracy is the most important, since it determines the arc a sensor expects to intercept the satellite on. In-track accuracy is generally less important, because it only affects how early or late the orbit will be along that arc. As Chapter III described, most observers set up an intercept position in advance of the pass and simply wait until the target appears.

Figure 5.8(a) shows the cross-track deviation of the computed orbit compared to the reference solution as it is propagated forward for nearly one day. Errors are greatest at $\pm 90°$ from the observation point, but pinch back together on the opposite side of the Earth. A more practical consideration is how likely an optical sensor could reacquire the target, but this is a function of observer-satellite geometry and the sensor itself. Since a sensor's field of view always plays a critical role, the right-hand axis in Figure 5.8(a) shows the equivalent angular separation of the predicted track from the satellite's true position, provided the satellite flew directly overhead. Therefore, not knowing any other parameters, Figure 5.8(a) indicates it could take up to a full 20° field of view to guarantee catching the satellite within the first day.

Just as cross track errors correspond in practice to angular deflections, in track errors are associated with the prediction's "lead" or "lag" of the actual satellite in time. Accordingly, both position errors and their equivalent timing errors are presented in Figure 5.8(b).

53

These figures are presented to aid additional analysis of telescope tracking networks. Although accuracy and precision of telescopes may vary, the fundamental trends presented here will probably remain present. Additional observations may negate this assessment: in the words of Norman Pogson, "but this I do not anticipate."
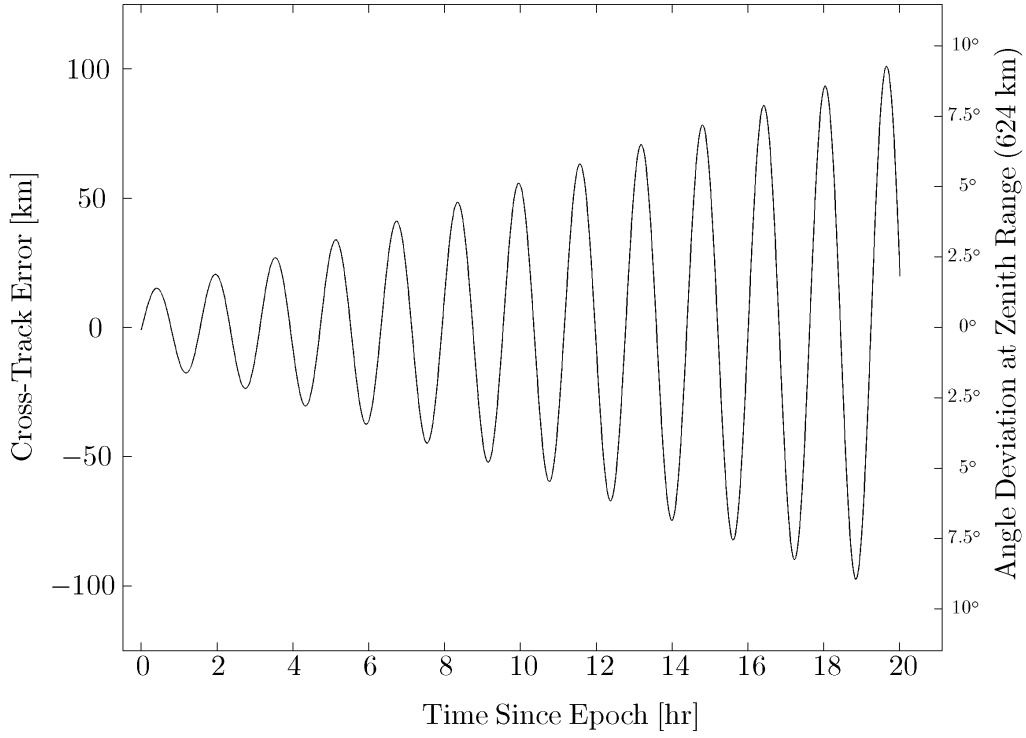
(a) Cross Track Errors of Computed Solution
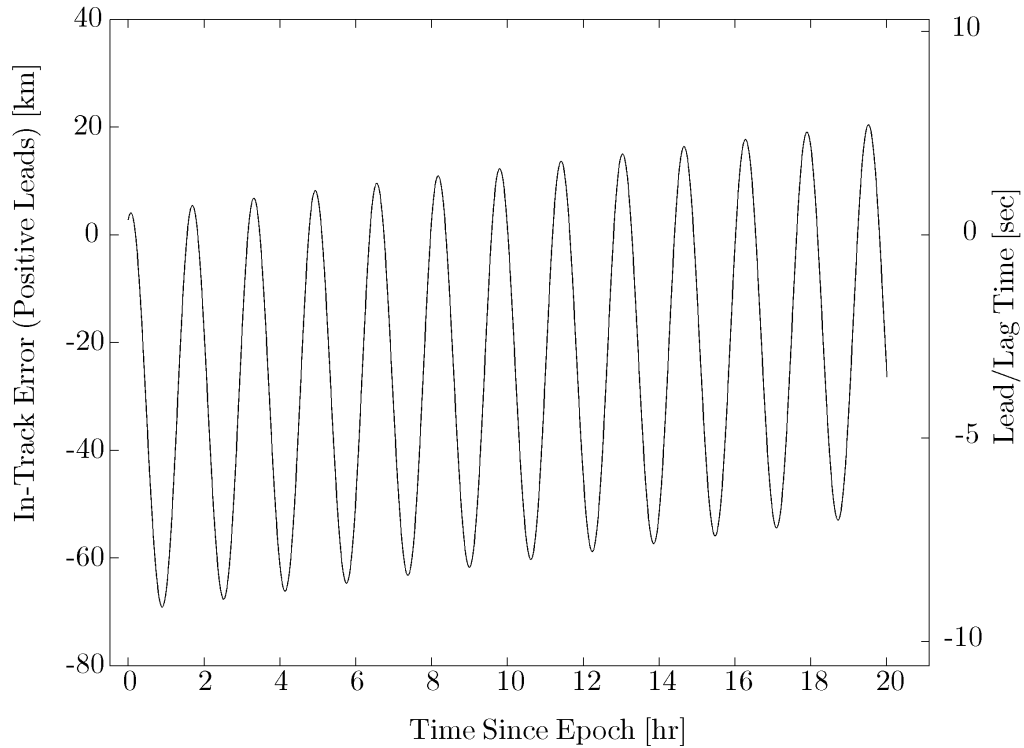
(b) In Track Errors of Computed Solution

Figure 5.8:   Cross Track and In Track Errors of Computed Solution

VI. Conclusions

ENVELOPES are important in research: engineers are either expanding them or designing on the back of one. The two activities are closely related. This paper is much like the proverbial envelope, covered in descriptions of the basic pieces required to assemble something much larger. It affirms many things that are established in theory, but often unfamiliar to most contemporary space professionals. There are other benefits to this back-to-basics approach as well. Just as great designs start out as simple scribbles, elementary success in this effort portends envelope-expanding capabilities.

Preliminary results answer the basic question offered at the outset, namely "is it possible to generate orbit predictions using commercial telescopes?" The short answer is yes, with the added benefit that doing so requires no special facilities and only a fractional budget (although weather can be problematic). This is only the first of many useful conclusions, however. Because the equipment is simple, even nontechnical individuals can participate in research. Volunteers with diverse backgrounds, rather than the author, usually operated the tracking software and found it fun and enlightening. These are exactly the emotions experienced by early Project Moonwatch volunteers, and it is rewarding to see echoes of that era. Whether the public ever contributes to satellite tracking with the widespread impact they once did remains to be seen, but it is exciting to imagine the implications. Nevertheless, sincere hopes are offered that the system developed here will at least help educate those without space experience and inspire new space-related research efforts.

Such research, when it occurs, should keep true to the goal of seeking elegant solutions using simple tools. There is a tendency to pursue bigger, better, faster, or more capable systems without pausing to consider why they are necessary. It is also easy to overemphasize theory and sacrifice tradecraft in the process. Working on a system like this one provides a natural counterbalance: if solutions become too theoretical in nature, they are no longer useful. Likewise, as errors or data trends are unearthed, an incessant stream of new theory is required to explain them. If future researchers do not stray too far from this locus, they can guarantee that any obtained results will be of practical use.

For these reasons, improving this tracking system or expanding its capabilities is a worthy effort. Various advances are achievable within the time and effort appropriate for graduate study. These efforts could include the following:

- Orbit/Observer Analysis: As it stands, there is not a complete analytic expression for great circle deviation ζ_{GC} as a function of orbit and groundsite parameters.[1] Although the author prefers this measurement-derived figure of merit, there are other methods that accomplish the same thing (refer to the discussion of singular matrices in ??). Regardless of the selected approach, it appears higher-elevation passes are less desirable. Without a more complete analysis of the behavior of either it is very difficult to optimize groundsite configuration for initial orbit determination.

- Space Operations: Inherent weaknesses in single-site observing can be negated with the application of binocular tracking, where at least two cameras track a target to triangulate range. It is an excellent operations optimization problem, which requires broad but basic modeling of tracking capability as a function of satellite brightness, sensor quality and placement, targeted satellite orbits, weather, et cetera.

- Optics and Remote Sensing: The camera used in this project was selected out of convenience. A better camera, or more likely a cluster of cameras could significantly improve LEO observations. A true optical "fence" with at least a 20° field of view would be a welcome development.

- Image Processing: Automatic target identification techniques could render manual postprocessing obsolete. This enables both large collection volume and possibly realtime solutions, which has obvious benefits for SSA missions.

- Systems Engineering: Naturally, the critical component in any future work is effective systems engineering. A more detailed systems-level analysis of the previously mentioned elements would ensure any future systems meet user requirements and are both sustainable and interoperable.

---

[1]References to this phenomena are more likely to be found in archives that contemporary journals. Moulton's derivation was published in 1914, and ground-based angles only techniques for LEO satellites are long out of vogue.

It goes without saying that any one of these contributions provides an excellent professional development opportunity, especially for those working in space-related fields. A multidisciplinary team would encounter many of the challenges faced by operators today, albeit in a much lower risk environment and with much greater personal control over system development. This work proves exciting not because it bring revolutionary new capability. Instead, the revolution fights to reinvigorate old concepts using effective and inexpensive new technology.

Appendix A. The Meade LX200GPS Telescope

THIS appendix presents a few details unique to working with the Meade LX200GPS telescope. They are not relevant to satellite tracking in general, but are presented here to aid future researchers. Four main issues are discussed here:

- Complications using the onboard GPS receiver: In its factory condition, the telescope is not able to provide entirely useful data to the personal computer.

- Discrepancies in attitude reporting: Although the telescope has a reported whole-sky targeting accuracy of two arcminutes ($\approx 0.03°$), there are barriers to extracting attitude information with the same quality.

- Control algorithm: To accomplish slew-and-shoot tracking, an estimate of the mount's speed is required.

- Imaging through the main optics: The 10" telescope optics were unused in this project because, when used with the selected camera, only a 1° field of view could be obtained. This was deemed too narrow for the purposes of the project, but some brief notes on pursuing this are included.

The Meade telescope used here has a built-in GPS receiver. Over the years, the actual chip used varies: this one uses a Sony GXB5210 in particular (discovered through careful dissection). The chip itself is designed to output standard National Maritime Electronics Association (NMEA) navigation messages. However, the chip is subordinate to the telescope's computer, so there are a few negative effects:

- Message Filtering: The telescope only uses the GPRMC message type to synchronize its computer. This message effectively contains UTC time, latitude, and longitude data only. Also, the computer filters all other messages, so it only provides GPRMC messages to the user over the RS232 port in its factory condition. Richard Seymour is a prolific publisher on Meade telescope firmware, and provides firmware patches that override this limitation and fix many other errors. His site also contains more detailed explanations of GPS navigation messages [*Seymour*, 2008b]. Using his 4.2g software patch, available at [*Seymour*, 2008c], it is possible to gain access to whatever NMEA messages the receiver is willing to provide.

- Message Availability: Depending on the chip's configured baud rate, only certain NMEA messages are broadcast:

> The GXB5210 can output 8 different types of sentence: GPGGA, GPGLL, GPGSA, GPGSV, GPRMC, GPVTG, GPZDA and PSGSA. If 9600bps or 19200bps or 38400bps baud rate is set for port setting, it outputs 7 types of sentence: GPGGA, GPGSA, GPGSV, GPRMC, GPVTG, GPZDA, PSGSA as default. Moreover, if 4800bps baud rate is set, it outputs 4 types of sentences: GPGGA, GPGSA, GPGSV, GPRMC as default. [*Sony Corporation*, Undated]

The telescope has the receiver chip hard-wired to 4800 baud, so with the 4.2g patch the GPGGA message may be used as well. Reading this message allows altitude determination. However, unless patch wires were soldered onto the control board and appropriate firmware changes made, it is not possible to gain access to the GPZDA message, which would provide UTC day/month/year info as well [*Seymour*, 2008a]. Therefore, in its current configuration, the user must ensure the personal computer is set to the correct UTC day, since the telescope cannot provide this information.

- Lag and Precision Issues: Probably due to a lag in the telescope's computer, GPS messages are not streamed sufficiently fast to be considered realtime. Comparisons of logfiles' mean determinations with their deviations show errors as high as 1.5 ± 0.009 seconds. A working correction of 1.5 seconds is now added to synchronization routines, but if greater timing precision is required it is recommended to abandon use of the onboard receiver.

In order to target the camera and record critical metadata for the measurement process, the telescope's computer must be able to slew to and accurately record any position from horizon to horizon. The computer is optimized to handle only the former. It takes a desired target, usually a Right Ascension (RA, α) and Declination (Dec, δ) value from a celestial object catalog, and corrects for measured tip, tilt, precession, nutation, and refraction effects.

In early attempts at pointing the telescope, GoTo Az and GoTo El targets were commanded (: $Sz\#$ and : $Sa\#$ in the Meade Command Protocol). The inverse measure-

ments (: $GZ\#$ and : $SA\#$) were recorded with videos. This corresponds to the *terrestrial* tracking mode, where the computer does not automatically engage sidereal tracking after each slew is complete. Apparently, it does not account for tip or tilt, either. To counter this, an attempt was made at back-calculating azimuth and elevation from the telescope's reported RA, Dec, computed LAST, and navigational data using transformations from [*Escobal*, 1965]. When working in RA and Dec coordinates, the telescope assumes *celestial* tracking mode, and automatically applies a number of corrections, as well as automatically engaging sidereal tracking after every slew.

In the following experiment comparing the az-el versus RA/Dec methods, interesting trends are noted. The telescope was carefully leveled (a carpenter's level was placed on the OTA through full travel) and slewed in a complete arc at 0°, 45°, and 85°, respectively. Figure A.1 shows the results.
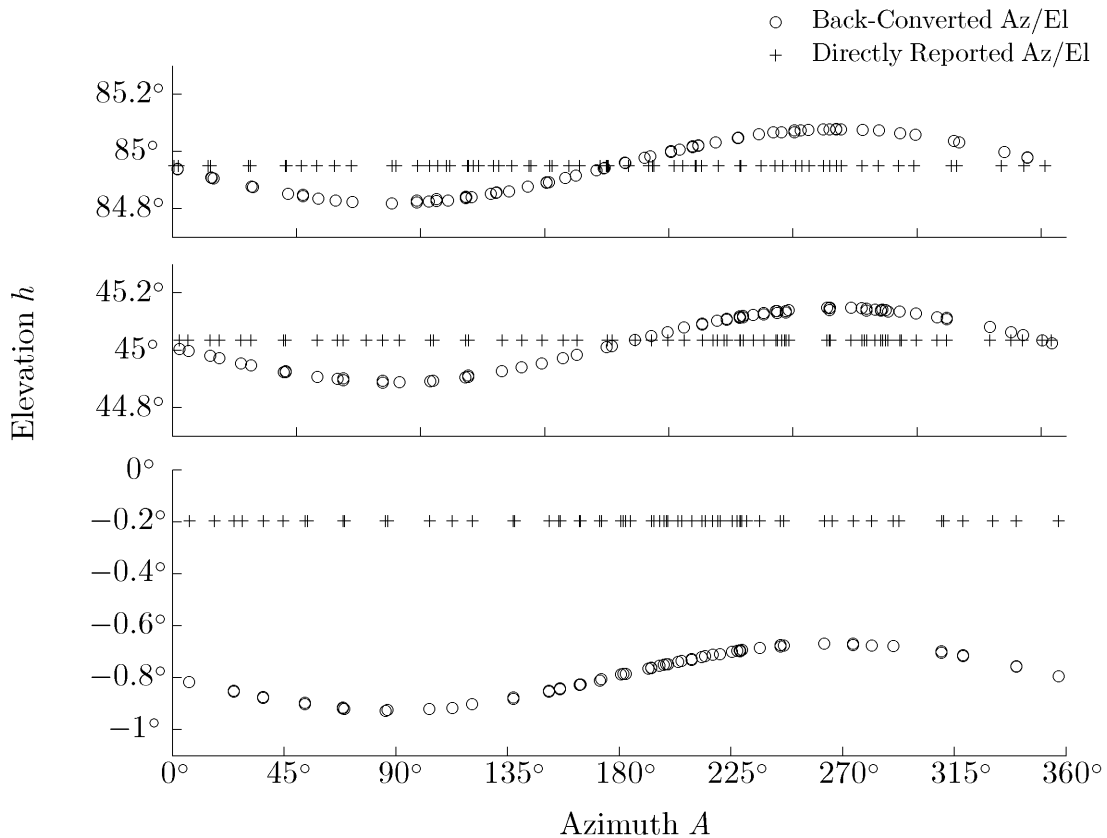

Figure A.1:   Back-Calculated and Directly Reported Azimuth and Elevation

61

These trends imply a few things. First, the scope *may* be subtracting refraction effects in its output position using the RA/Dec method.[1] The sine trend could be due to multiple things:

- LAST Miscalculation: Many observers note their telescope's computation of LAST differs from what it should be (Richard Seymour confirms there are both past and current examples of this). This would result in a net "twist" in results.

- Invisible Precession/Nutation/Tip-Tilt Parameters: Richard Seymour also confirms that the computer uses its own internal coordinate reference frame, which is generally unavailable to the user. It is possible this twist is due to rotations caused by "invisible" parameters such as precession, tip, and tilt.[2]

These issues may not need resolution, however, because the RA/Dec method turns out to be much slower than the az-el one. Furthermore, it is harder to predict how long a slew will take, because the telescope overshoots the target, then approaches it in the sidereal tracking direction to avoid gear backlash issues. This is excellent for observing stars, but detrimental to satellite tracking, since it results in lost observing time.

Speaking of observing time, the slew-and-shoot technique requires an estimate of how long it takes the telescope to move from any arbitrary point to any other. Lab tests revealed that, when powered by an external supply, a commanded slew moves at a fairly linear $4.7\frac{\circ}{sec}$ in both axes. This is preceded by a two second command delay, and roughly a six second settling time. These estimates are working well in practice, since the telescope will reach its intended target (usually a five second lead in the satellite track) and settles out consistently. The one issue not yet addressed is the occasional "unwinding" that occurs when the telescope computer decides to move its azimuth axis closer to home position (this axis has $\pm 360°$ net travel). A running tally of slews could be kept in the software to predict when such a move is likely.

To date, the original az-el method is being used. By leveling the telescope a little more carefully, and using only measurements with reference stars in them, reliable re-

---

[1] At the horizon, exo-atmospheric objects appear $\approx 0.5°$ higher than they actually are.

[2] It is possible failure to correctly apply the equation of the equinoxes is at fault, a fact discovered shortly before publication.

sults may be obtained. Subsequent researchers will undoubtedly resolve any outstanding issues.

Finally, an all-too-common question is: "why do you have that big telescope if you don't use it?" The answer is simple: a) buying the mount and telescope separately isn't cost effective, b) the main optics still enable precise alignment, and c) it may be used in later projects. The current camera was tested with a Meade f/3.3 focal reducer to determine what kind of images could be expected.[3] Image quality was similar to those produced with the SLR lens, but the field of view was on the order of 1°. It was deemed unsuitable for this first research attempt, but is certainly worth employing for appropriate projects, such as satellite tracking in higher orbits. Better cameras should definitely be employed whenever possible, as well.

---

[3]A focal reducer is a specially-crafted lens that effectively shortens the focal length of the telescope, which gives it a wider field of view (to offset magnification caused by small CCDs) and focuses more light on each pixel, resulting in faster exposures.

Appendix B. MATLAB® Function Descriptions

N UMEROUS MATLAB® scripts and functions are used in the course of this research project. This appendix is divided into four parts: one each for the target identification script, integrated tracking software, measurement software, and angles only orbit determination tools. Since there are numerous inputs and outputs, most of which are graphics handles, these are omitted for clarity.

B.1 Target Identification Script

This script performs all calculations presented in Chapter III. A user must provide the following input files:

- **NORAD Three-Line Element Set**: The three-line version of a NORAD element set includes the satellite's common name on the line preceding the two-line data set. Operators always want to know what they're tracking. These are available from celestrak.com, with filename format *catalog_3l_YYYY_MM_DD_am.txt* or *catalog_3l_YYYY_MM_DD_pm.txt*, depending if it is the morning or evening (Colorado time) catalog release.

- **qs.mag**: This is Mike McCants' intrinsic satellite brightness catalog, posted at [*McCants*, 2008c].

- **mcnames**: The original Ted Molczan catalog, available at the same location just referenced.

- **ha.txt**: An intrinsic brightness file generated from the satellite database at *Heavens Above* [*Peat*, 2008].

- **sun.txt**: Solar ECI vectors from JPL's HORIZONS website [*JPL*, 2008]. Data must be extracted with the following options:

    - Ephemeris Type: VECTORS

    - Target Body: Sun [Sol] [10] (note planets could be added to the current star chart substituting planetary data here)

    - Coordinate Origin: GEOCENTRIC (500) (i.e. ECI)

64

– Time Span: Choose any span (current file valid through 2008), but TIME STEP = 1d (starting at UTC 00:00:00).

– Table Settings: Output Units = $KM\&KM/d$

– Quantities Code= 2 (State Vector: x,y,z,vx,vy,vz)

– Reference Units: Earth mean equator and equinox of reference epoch.

– Reference System: ICRF/J2000.0

– Correction: None

– Labels: Disabled

– CSV Format: Disabled

– Display/Output: Download/Save (this generates an output .txt file).

Using this or equivalent source data, the following output files are generated:

- **precalc_results.mat**: This contains results of brightness calculations. Its most notable variable is *obs_keep*, which lists satellite brightness as a function of JD. Only satellites that beat a minimum threshold *at one point* during the selected timespan (usually sunset to sunrise). Dim passes are filtered by the integrated tracking software. Any time the satellite is below the horizon, its brightness is listed as "99."

- **precalc_tle.txt**: This file is unused by later scripts, but is a trimmed three-line catalog containing only a) satellites with periods less than some desired number (225 minutes is the default for LEO) and b) only satellites with brightness data in one of the three catalogs listed above.

- **QUICKSAT.DAT**: This is a Quicksat-friendly element set file including only bright satellite ephemerides. Quicksat uses non-Windows carriage returns and has a maximum catalog input of 3000 satellites [*McCants*, 2008a].

There are many scripts used to process these inputs and save outputs, most of which are inherent to core `MATLAB`® code or its Aerospace or Mapping Toolboxes. Notable ones include:

- Vectorized SGP4 Scripts: The following are vectorized versions of Jeff Beck's `MATLAB`® adaptation of David Vallado's SGP4 code written in C. The complete package may be found at [*Kelso*, 2007]. Note only the following files are modified, but they may still depend on subfunctions included in the referenced collection. These scripts in concert produce $\vec{r}_{sat}$.

    - **dpper_vectorized.m**: Modified for vector output.

    - **dspace_vectorized.m**: Modified for vector output.

    - **sgp4_vectorized.m**: Core SGP4 code.

    - **sgp4_init_vectorized.m**: Minor change, now points to _vectorized versions of code so originals may be deleted.

    - **twoline2rv_simple.m**: Corrects a number of errors and produces initial orbital elements and epoch times for a single satellite at a time, given two-line input strings from the catalog.

- **getcatalogsats.m**: Using input data, produces precalc_tle.txt.

- **getdarkness.m**: Computes sunrise and sunset times.

- **getstars.m**: Imports data from the Yale Bright Star catalog and produces a table of star identifier, right ascension, declination, and apparent magnitude.

- **getsite.m**: Calculates the site's ECI position vector, $\vec{r}_{site}$.

- **getsun.m**: Extracts ECI sun vectors from sun.txt, then interpolates them as necessary to get $\vec{r}_{Sun}$.

- **getzenith.m**: Calculates the site's zenith vector in ECI coordinates.

B.2   *Integrated Tracking Software*

The integrated tracking software is shown in Figure 3.2. By default, it refreshes all data at a set rate (currently 15 seconds) unless otherwise noted. For certain operations,

it automatically places important information in a file named **logfile.txt**. This Graphic User Interface (GUI) has the following features:

- Comprehensive Starmap: The upper-left corner features a starmap that shows not only the current position of numerous bright stars, but also target satellite paths, the telescope's current position, and the telescope's intercept position.

- Brightness Predictions and Satellite Targeting: Results stored in *precalc_results.mat* may be viewed graphically in the screen's lower left corner. For any given minute (the default precalculation step size), a satellite's expected brightness is indicated with one of six bar intensities, one each for apparent magnitudes above six. Currently, satellites are sorted so those with the highest mean brightness in the next 15 minutes are at the top. By clicking on any satellite, it is automatically targeted. When targeted, a) the satellite path is shown on the starmap in the upper left corner, b) a telescope slew is generated along with an estimated time of travel, and c) a countdown to the time the satellite will cross the image center begins. Slots are reserved for any satellite becoming visible in the next 25 minutes, but they are only shown if rising in the next 15 minutes.[1] If a satellite is not yet risen, an arrow indicates the direction of its pass. Once a satellite is overhead, its future path is shown in red, its current position is marked with a square, and its location within the last five minutes is shown in gray.

- Guide Star Targeting and Identification: The "Stars" button brings up a menu of currently visible guide stars (stars that the Meade telescope uses in its alignment process). Selecting one initiates the same process as with satellites, except the star changes color on the starmap instead of producing an overflight path. This feature helps non-astronomers find requested stars when asked for them by the Meade computer. It is also useful for checking telescope alignment and recording calibration videos.

- Video Preview and Recording: The upper right-hand corner shows a preview of the camera video, with a central crosshair superimposed over it. Immediately below

---

[1]Reserving slots prevents the chart from becoming to "jumpy" as new sats appear. Otherwise, a satellite's ranking may change rapidly.

it, a box displays the UTC time a satellite is expected to cross the image center (assuming the telescope reaches intercept by its predicted time), a countdown to the same time, and a "Record" button that logs both streaming video and relevant metadata to the logfile.[2]

- Telescope Slew Controls and Data Readout: A text output of selected target, estimated time to intercept, current telescope position, and intercept telescope position is shown below the video recording box. The Slew command button initiates an immediate recalculation of all orbit and intercept geometries, commands the telescope to slew, and automatically deselects the button when a slew is complete (once the telescope reports the same position for three consecutive seconds). The Track and Sync buttons are mutually exclusive.

- Location Information: As a check, location information is provided in the lower-right hand corner. The Sync button initiates a synchronization routine with the telescope's onboard computer. It also logs raw GPS message data to the logfile. The Sync and Track buttons are mutually exclusive.

- Time Selection Box: Normally, the software is used in realtime, which requires selecting the Current Time radio button. To view any other time, the operator may select User Selected Time, which allows examination of scenarios in the past or future. Typically, this feature is used to look ahead during a sortie to find out if suitable targets still remain.

As before, numerous functions are required to generate the GUI and process user inputs. Significant scripts include:

- **trackgui.m**: Master script, generates the majority of interface objects and execution timers.

- **refreshgui.m**: Triggers GUI update on a set refresh cycle.

- **createschedule.m**: Generates the brightness data strip chart and triggers target-related updates when a satellite is selected from the plot.

---

[2]The "Auto" label refers to an unimplemented feature that automatically begins logging video when the countdown timer reaches a set threshold.

- **createstarmap.m**: Computes expected positions of visible stars and plots them on the starmap.

- **buildsattrack.m**:Recalculates the expected time, azimuth, and elevation of a satellite overflight and plots its path on the starmap.

- **findtelescope.m**: Queries available ports for an active Meade telescope, then automatically connects if one is found.

- **getscopeposition.m**: Queries the telescope for its current position. If errors are encountered, it generates a "No Scope" error in the tracking software.

- **gpssync.m**: Imports the telescope's GPS data stream and logs relevant navigational data. It runs a comparison of the reported stream time with the computer's own clock, then notes the offset. If the standard deviation is sufficiently low, the tracking software applies this offset to all subsequent time calculations and displays. If not, a warning occurs. If other errors are encountered, it generates a "No Scope" error in the tracking software.

- **slew.mcancelslew.m**: Initiates or cancels telescope slewing while employing a number of crosschecks. If errors are encountered, each generates a "No Scope" error in the tracking software.

- **slewbuilder.m**: Given a current telescope location and a targeted satellite, this function estimates the approximate travel time required. It then returns a target intercept position and estimated time the satellite will cross image center.

B.3 Video Measurement Software

Video measurement software, shown in Figure 4.3, allows a user to import collected videos, correct for misalignments, and measure satellite streaks. It automatically reads logfile.txt, generated with the integrated tracking software during observations. Once it imports the metadata associated with each video (and if every piece of critical metadata is present), the software calculates the expected position of any visible stars and displays them directly on the video. A Show Stars checkbox removes computer-predicted guide star locations. Using controls on the right, corrections for azimuth, elevation, and camera

twist are interactively applied. Once this step is complete, a user need only click on the satellite streak to generate a JD time, azimuth, and elevation record under the "measurement" variable.

Major scripts and functions include:

- **measurevideo.m**: Main script that generates the GUI and defines all button callback functions.

- **getstars.m**: As previously described. Assumed epoch is the computer date/time, stars are trimmed to apparent magnitude six and above by default. This function runs only once at script startup.

- **loadvideo.m**: Imports video data, erases bad pixels by matching their intensities to the frame mean, and identifies corresponding metadata from the logfile.

- **getstarazel.m**: Converts stars' ECI pointing vectors from getstars.m to the SEZ frame using each video's metadata, then trims all results to only those stars above the horizon after accounting for generic atmospheric refraction. Repeats on each frame refresh, allowing the stars to drift at their appropriate rates (assuming a stationary camera). Currently, *every* star is transformed in this step, because no serious delays are observed.

- **buildfovstars.m**: Further trims stars to include only those that will appear in the URD frame (i.e. the video), determines their corresponding locations in pixels, then plots and labels them on the video.

- **measureimage.m**: Whenever the video is clicked, this function identifies the pixel clicked, converts it to a corresponding URD pointing vector, corrects it using the azimuth, elevation, and twist errors identified earlier, transforms it to the SEZ frame, then unrefracts it to an airless measurement.

B.4   Angles Only Orbit Determination Tools

Once airless JD time, azimuth, and elevation measurements are available from the measurement software, they may be used in conjunction with site parameters to produce

topocentric pointing vectors and subsequent orbit solutions. A few variations of scripts are used to not only determine initial orbits, but also analyze and interpret results. This section describes the baseline deterministic configuration: measurements are used directly, so no uncertainty is generated. The entire method follows from [*Vallado and Mc-Clain*, 2007], which should be consulted for details. This script **measureconverter.m** requires the following inputs:

- **measurement**: This variable is produced using the video measurement software. It is typically imported from NNNNN.mat, a workspace file containing the measurement variable for a given satellite ID.

- **azelrange**: This variable is the result of using the satpath.m script, which is a version of precalcs.m that computes observation geometry for only one satellite. It is a table of JD times with a corresponding azimuth and elevation for each. This variable allows error calculations and a display of "true" results for comparisons. Otherwise, it is unnecessary.

Given these inputs, the script automatically selects measurements to produce the topocentric pointing vectors $\hat{\vec{l}}_{first}$, $\hat{\vec{l}}_{mid}$, and $\hat{\vec{l}}_{last}$. Calculations proceed as previously described.

Appendix C. Select Satellite Observations

I N the course of three sorties, the following satellites were tracked. Site parameters for all observations are listed in Table C.

Table C.1:   Site Parameters for Select Observations

Geodetic Latitude ϕ:	39.6802° (North)
Geodetic East Longitude λ_E:	−83.8383° (West)
Height Above Geoid H:	287.6 [m]

Table C.2:   Select Satellite Observations

Satellite Name (NORAD ID)	Observation Times	Azimuth	Elevation
THOR AGENA D R/B (733)	16-Jan-2008 10:59:00Z	220.76	60.26
	16-Jan-2008 10:59:38Z	211.08	46.35
	16-Jan-2008 11:00:19Z	206.61	34.78
COSMOS 1812 (17295)	28-Jan-2008 00:08:26Z	66.89	57.58
	28-Jan-2008 00:09:10Z	115.15	53.09
	28-Jan-2008 00:09:17Z	120.51	51.01
COSMOS 1825 (17566)	28-Jan-2008 00:24:37Z	321.66	47.38
	28-Jan-2008 00:25:21Z	340.87	34.07
	28-Jan-2008 00:26:05Z	349.80	24.02
SL-14 R/B (18215)	03-Feb-2008 00:26:16Z	28.96	43.72
	03-Feb-2008 00:28:32Z	133.73	42.25
	03-Feb-2008 00:30:33Z	155.72	17.54
SL-3 R/B (19046)	28-Jan-2008 00:11:11Z	162.70	68.06
	28-Jan-2008 00:12:42Z	348.73	50.64
	28-Jan-2008 00:13:59Z	347.90	25.78
SL-16 R/B (19120)	16-Jan-2008 10:49:52Z	302.56	81.97
	16-Jan-2008 10:50:34Z	176.08	75.15
	16-Jan-2008 10:51:16Z	166.06	57.62
COSMOS 1980 (19649)	03-Feb-2008 00:37:13Z	172.87	45.03
	03-Feb-2008 00:39:15Z	84.62	64.87
	03-Feb-2008 00:40:33Z	45.42	44.52

Table C.3:   Select Satellite Observations, Continued

Satellite Name (NORAD ID)	Observation Times	Azimuth	Elevation
SL-8 R/B (20433)	16-Jan-2008 11:03:26Z	184.16	59.07
	16-Jan-2008 11:04:45Z	51.03	76.60
	16-Jan-2008 11:05:27Z	29.67	57.59
ERS 1 (21574)	28-Jan-2008 00:39:27Z	65.50	51.17
	28-Jan-2008 00:40:00Z	44.54	47.67
	28-Jan-2008 00:40:10Z	39.38	46.01
UARS (21701)	03-Feb-2008 00:43:11Z	203.98	29.90
	03-Feb-2008 00:43:20Z	202.30	32.68
	03-Feb-2008 00:43:51Z	192.70	45.00
COSMOS 2219 (22219)	16-Jan-2008 10:38:19Z	91.94	55.35
	16-Jan-2008 10:38:55Z	70.96	49.89
	16-Jan-2008 10:39:03Z	67.28	48.29
SL-14 R/B (22287)	16-Jan-2008 10:56:33Z	112.03	73.84
	16-Jan-2008 10:56:34Z	114.68	73.25
	16-Jan-2008 10:56:36Z	117.28	72.91
SL-16 R/B (23088)	03-Feb-2008 00:11:45Z	70.01	29.44
	03-Feb-2008 00:12:44Z	86.91	25.91
	03-Feb-2008 00:13:27Z	96.60	22.49
SL-16 R/B (23705)	16-Jan-2008 11:26:45Z	349.90	31.36
	16-Jan-2008 11:27:25Z	354.70	39.84
	16-Jan-2008 11:28:24Z	9.75	55.93
COSMOS 2333 (24297)	03-Feb-2008 00:46:23Z	136.29	43.73
	03-Feb-2008 00:46:31Z	2454499.53	132.46
	03-Feb-2008 00:47:06Z	114.45	47.87
SL-8 R/B (27535)	28-Jan-2008 00:34:22Z	96.58	45.62
	28-Jan-2008 00:34:56Z	110.05	42.07
	28-Jan-2008 00:35:00Z	111.40	41.60
SL-16 R/B (28353)	03-Feb-2008 01:06:54Z	171.70	47.70
	03-Feb-2008 01:07:03Z	169.18	50.16
	03-Feb-2008 01:07:37Z	153.93	60.02
CZ-4B R/B (29093)	03-Feb-2008 00:58:29Z	328.46	33.16
	03-Feb-2008 00:58:37Z	330.14	30.80
	03-Feb-2008 00:59:09Z	334.82	23.23
SKYMED 1 (31598)	16-Jan-2008 11:14:45Z	146.73	61.92
	16-Jan-2008 11:15:59Z	9.40	66.05
	16-Jan-2008 11:16:42Z	357.03	45.87
SL-16 R/B (31793)	27-Jan-2008 23:55:57Z	40.12	53.91
	27-Jan-2008 23:57:19Z	30.74	32.81
	27-Jan-2008 23:59:16Z	26.94	15.96

Bibliography

Bate, R. R., D. D. Mueller, and J. E. White. *Fundamentals of Astrodynamics*. New York: Dover Publications, 1971.

British Broadcasting Corporation (BBC) Manchester. "Lovell Telescope: 50 Years On," 18 October 2007. 25 February 2008. http://www.bbc.co.uk/manchester/.

Culp, R. D., and I. J. Gravseth. "Space-Debris Identification Using Optical Calibration of Common Spacecraft Materials," *Journal of Spacecraft and Rockets, 33*(2), 262–266 (March-April 1996).

Dana, P. H. "Global Positioning System Overview," 1 May 2000. 25 February 2008. http://www.colorado.edu/geography/gcraft/notes/gps/gps_f.html.

Department of the Air Force. "Factsheets: Ground-Based Electro-Optical Deep Space Surveillance," November 2006. 1 February 2008. www.af.mil/factsheets/factsheet.asp?fsID=170.

Earl, M. "CASTOR: Canadian Satellite Tracking and Orbit Research," 9 February 2008. 14 February 2008. http://www.castor2.ca/index.html.

Engle, E., and K. H. Drummond. *Sky Rangers*. New York: John Day Company, 1965.

Escobal, P. R. *Methods of Orbit Determination*. New York: Wiley, 1965.

Harvard-Smithsonian Center for Astrophysics. "Australian Project Moonwatch Volunteers," Undated. 14 February 2008. Courtesy Christine Pulliam, Public Affairs Specialist.

Henize, K. G., M. K. Mulrooney, C. A. O'Neill, and P. Anz-Meador. "Optical Properties of Orbital Debris," *Journal of Spacecraft and Rockets, 31*(4), 671–677 (July-August 1994).

Hoffleit, E. D., and W. H. J. Warren. "The Bright Star Catalogue, 5th Revised Ed. (Preliminary Version)," 1991. September 2008. ftp://adc.gsfc.nasa.gov/pub/adc/archives/catalogs/5/5050/.

Hoots, F. R., R. L. Roehrich, and T. S. Kelso. "Spacetrack Report #3: Models for Propagation of NORAD Element Sets," 31 December 1988. 10 February 2008. http://celestrak.com/NORAD/documentation/spacetrk.pdf.

Jet Propulsion Laboratory (JPL). "HORIZONS System," 2008. 4 February 2008. http://ssd.jpl.nasa.gov/horizons.cgi.

Kaplan, G. H. "Circular Number 179: The IAU Resolutions on Astronomical Reference Systems, Time Scales, and Earth Rotation Models," 20 October 2005. 4 February 2008. http://aa.usno.navy.mil/publications/docs/Circular_179.pdf.

Kelso, T. S. "Revisiting Spacetrack Report #3," 5 July 2007. 4 February 2008. http://celestrak.com/publications/AIAA/2006-6753/.

Kennon, W. L. *Astronomy: A Textbook for Colleges*. Boston; New York; Chicago: Ginn and Company, 1948.

Kervin, P. W., J. L. Africano, P. F. Sydney, and D. Hall. "Small Satellite Characterization Technologies Applied to Orbital Debris," *Advances in Space Research, 35*(7), 1214–1225 (2005).

Matson, R. "Satellite Visual Magnitude Equations," 26 April 2001. 7 February 2008. http://www.satobs.org/seesat/Apr-2001/0313.html.

Matson, R. "Satellite Brightness Formulations," 7 February 2008. Personal Correspondence.

McCants, M. "A Few Program Files," 2008a. 15 February 2008. http://www.io.com/~mmccants/programs/index.html.

McCants, M. "Intrinsic Magnitude Definitions," 2008b. 15 February 2008. http://www.io.com/~mmccants/tles/intrmagdef.html.

McCants, M. "Mike McCants' Satellite Tracking TLE ZIP Files," 2008c. 15 February 2008. http://www.io.com/~mmccants/tles/.

Meade Corporation. "Meade Telescope Serial Command Protocol, Revision L," 9 October 2002. 2 February 2008. www.meade.com/support/LX200CommandSet.pdf.

Meeus, J. *Astronomical Algorithms.* Richmond, Va.: Willmann-Bell, 1998.

National Aeronautics and Space Administration (NASA). "Astronomy Picture of the Day: Sputnik 1," 4 October 2007. 12 February 2008. http://antwrp.gsfc.nasa.gov/apod/ap071004.html.

National Imagery and Mapping Agency (NIMA). "Department of Defense World Geodetic System 1984 (TR8350.2)," 3 January 2000. http://earth-info.nga.mil/GandG/publications/tr8350.2/wgs84fin.pdf.

Peat, C. "Heavens Above," 2008. 4 February 2008. http://www.heavens-above.com.

Pogson, N. "Magnitudes of Thirty-Six of the Minor Planets for the First Day of Each Month of the Year 1857," *Monthly Notices of the Royal Astronomical Society, 17*(1), 12–13 (14 November 1856).

Rees, G. *Physical Principles of Remote Sensing.* Cambridge, UK; New York: Cambridge University Press, 2001.

SeeSat-L User Group. "Satellite Observations: More Than Just Looking," February 1998. 4 February 2008. http://www.satobs.org/faq/Chapter-07.txt.

SeeSat-L User Group. "Iridium Flares," February 2007. 11 February 2008. http://satobs.org/iridium.html.

SeeSat-L User Group. "Bright Satellite Resources," Undated. 4 February 2008. http://www.satobs.org/brite.html.

Seymour, R. "LX200GPS Firmware Discussions," 2008a. 31 January 2008. Personal Correspondence.

Seymour, R. "Richard Seymour's Homepage," 2008b. 14 February 2008. http://rseymour.home.wolfenet.com/.

Seymour, R. "Richard Seymour's Homepage: Patches," 2008c. 14 February 2008. http://rseymour.home.wolfenet.com/patches/.

Smithsonian National Air & Space Museum. "Sputnik 1 - Milestones of Flight," . 1 February 2008. http://www.nasm.si.edu/exhibitions/GAL100/sputnik.html.

Sony Corporation. "GXB5210 GPS Receiver Datasheet," Undated. 12 February 2008. http://www.sony.co.jp/ semicon/english/img/sony01/a6808867.pdf.

Spiro, I. J., and M. Schlessinger. *Infrared Technology Fundamentals*. New York: Dekker, 1989.

Thrall, M. L. *Orbit Determination of Highly Eccentric Orbits Using a Raven Telescope*. MS thesis, Naval Postgraduate School (NPS), Monterrey, CA, September 2005 (ADA439558). http://handle.dtic.mil/100.2/ADA439558.

United States Naval Observatory. "Circular Number 163: The IAU Resolutions on Astronomical Constants, Time Scales, and the Fundamental Reference Frame," 10 December 1981. 5 February 2008. http://aa.usno.navy.mil/publications/docs/Circular_163.pdf.

United States Naval Observatory. "Rise, Set, and Twilight Definitions," 14 September 2007a. 5 February 2008. http://aa.usno.navy.mil/faq/docs/RST_defs.php.

United States Naval Observatory. "Approximate Sidereal Time," 14 September 2007b. 3 February 2008. http://aa.usno.navy.mil/faq/docs/GAST.php.

Vallado, D. A., and W. D. McClain. *Fundamentals of Astrodynamics and Applications*. El Segundo, CA; Boston: Microcosm Press, 2007.

Vallado, D. A., P. Crawford, R. Hujsak, and T. S. Kelso. "Revisiting Spacetrack Report #3 (AIAA 2006-6753)," *AIAA/AAS Astrodynamics Specialist Conference and Exhibit* (21 - 24 August 2006) http://celestrak.com/publications/AIAA/2006-6753/AIAA-2006-6753.pdf.

Whipple, F. L., and J. A. Hynek. "A Research Program Based on the Optical Tracking of Artificial Earth Satellites," *Proceedings of the Institute of Radio Engineers, 44* (6), 760–764 (June 1956).

Wiesel, W. E. *Modern Orbit Determination*. Beavercreek, OH: Aphelion Press, 2003.

REPORT DOCUMENTATION PAGE

1. REPORT DATE *(DD-MM-YYYY)*	2. REPORT TYPE	3. DATES COVERED *(From - To)*
01-03-2008	Master's Thesis	Sep 2007 - Mar 2008

4. TITLE AND SUBTITLE

Initial Determination of Low Earth Orbits Using Commercial Telescopes

5a. CONTRACT NUMBER

5b. GRANT NUMBER

5c. PROGRAM ELEMENT NUMBER

6. AUTHOR(S)

Schmunk, Matthew, M., Captain, USAF

5d. PROJECT NUMBER

5e. TASK NUMBER

5f. WORK UNIT NUMBER

7. PERFORMING ORGANIZATION NAME(S) AND ADDRESS(ES)

Air Force Institute of Technology
Graduate School of Engineering and Management (AFIT/EN)
2950 Hobson Way
WPAFB OH 45433-7765

8. PERFORMING ORGANIZATION REPORT NUMBER

AFIT/GA/ENY/08-M11

9. SPONSORING/MONITORING AGENCY NAME(S) AND ADDRESS(ES)

N/A

10. SPONSOR/MONITOR'S ACRONYM(S)

11. SPONSOR/MONITOR'S REPORT NUMBER(S)

12. DISTRIBUTION/AVAILABILITY STATEMENT

APPROVED FOR PUBLIC RELEASE; DISTRIBUTION UNLIMITED

13. SUPPLEMENTARY NOTES

14. ABSTRACT

Within the last decade, many new technologies have significantly changed the face of private astronomy. Developments such as inexpensive but high-quality sensors, rapid personal computing, and easy networking inspire a reexamination of an old problem: how practical is it to develop initial orbit estimates for Low Earth Orbiting (LEO) satellites using optical tracking? This paper documents the design and implementation of a commercial telescope system used to answer precisely that question. This analysis determined there are some challenging barriers to successful single-site orbit determination, but it is possible given the right conditions. Considering the low cost and small support footprint of such systems, they could provide excellent support to Space Situational Awareness (SSA) missions or satellite tracking operations in general.

15. SUBJECT TERMS

Astronomical Cameras, Brightness, Low Orbit Trajectories, Orbits, Satellite Tracking Systems, Satellites (Artificial), Space Surveillance, Spacecraft Debris, Telescopes, Tracking Telescopes

16. SECURITY CLASSIFICATION OF:			17. LIMITATION OF ABSTRACT	18. NUMBER OF PAGES	19a. NAME OF RESPONSIBLE PERSON
a. REPORT	b. ABSTRACT	c. THIS PAGE			Richard G. Cobb (ENY)
U	U	U	UU	90	19b. TELEPHONE NUMBER *(Include area code)* (937) 255-6565 x4559; Richard.Cobb@afit.edu